Coastal Engineering 63 (2012) 62–80

Contents lists available at SciVerse ScienceDirect

Coastal Engineering

journal homepage: www.elsevier.com/locate/coastaleng

Modelling gravel barrier profile response to combined waves and tides using XBeach: Laboratory and field results

Jon J. Williams [a,*], Amaia Ruiz de Alegría-Arzaburu [b,1], Robert T. McCall [c], Ap Van Dongeren [d,2]

[a] ABPmer, Suite B, Town Quay, Southampton SO14 2AQ, UK
[b] Instituto de Ingeniería, Universidad Nacional Autónoma de México, Edificio 5, 2do.Piso, Cubículo 307, Ciudad Universitaria, Coyoacán, 04510, México D.F, Mexico
[c] School of Marine Science and Engineering, University of Plymouth, Plymouth, PL4 8AA, UK
[d] Deltares, Postbus 177, 2600 MH Delft Delft, Netherlands

ARTICLE INFO

Available online 24 January 2012

Keywords:
XBeach model
Gravel barrier
Overwash
Storm impact
Threshold

ABSTRACT

XBeach, a process-based numerical model capable of computing nearshore circulation and morphodynamics, including overwash and breaching, has been used in 1D mode to simulate erosion occurring on a gravel barrier beach (D_{50} = 11 mm) subjected to wave and tidal forcing during selected tests undertaken during the BARDEX experiments. The model demonstrated good quantitative skill (Brier skill score, BSS, typically 0.65) with respect to beach face erosion, offshore accretion and morphological impacts of washover. XBeach was also used to model storm impacts on a steep (average tanβ = 0.12), 4.5 km-long and 100 m–140 m wide macrotidal gravel barrier (D_{50} = 2 mm to 10 mm) located in SW England. Although the development of a storm berm was not reproduced well, erosion was predicted with sufficient skill (BSS = 0.60) to meet practical engineering requirements concerned with predicting storm impacts and threshold wave and water level conditions for gravel barrier overwashing.

1. Introduction

Erosion and overwashing of gravel beaches and barriers can occur during storms and can lead to breaching and coastal flooding in the most extreme cases (cf. Bradbury and Powell, 1992; Bradbury et al., 2005; Pye, 2001; Pye and Blott, 2009). In order to predict and plan for storm impacts, coastal managers require a reliable model that enables identification of vulnerable areas, and assists with implementing effective coastal defence strategies. Past attempts to quantitatively predict and simulate overwash have met with limited success and only now are new tools emerging that appear to offer a better solution, (Donnelly et al., 2006).

Most recent modelling efforts have focussed on predicting the morphological response of sandy beaches. Notable progress in this area has been made by Srinivas and Dean (1996), who developed a 1D-cross shore numerical model with the capacity to simulate washover due to overtopping flow, and by Larson and Kraus (1989), with the field validated SBEACH model, and by Stockdon et al. (2007), who examine hurricane impacts. The quasi-2DV cross shore profile model UNIBEST-TC (Bosboom et al., 2000; Roelvink and Stive, 1989; Stive and Wind, 1986) has been adapted by Tuan et al. (2006) to include wave overwash and found to simulate morphological development with some skill. The 2DH model XBeach has been successfully applied to simulate erosion and overwash on two sandy barrier islands in the United States (McCall et al., 2010; Roelvink et al., 2009).

Using data from scaled laboratory experiments, the first parametric models developed for prediction of gravel beach morphology have focussed on cross-shore beach response to wave forcing and include: BREAKWAT, Van der Meer (1988); and SHINGLE, (Powell, 1990). Beach profile changes predicted by these models are governed by changes in wave height, wave period, wave duration, beach material and angle of wave attack. In their original form these models were unable to simulate barrier overwash and breaching, and thus Bradbury and Powell (1992) added a freeboard parameter to SHINGLE to account for these processes. The SHINGLE model was further modified by Bradbury (2000) to enable the prediction of the threshold conditions for barrier breaching, thus addressing a fundamental design requirement for gravel beach nourishment and restoration projects. It was found however, that the model was rather site dependant and tended to under predict overwash for beaches at other locations (cf. Bradbury et al., 2005). This issue was addressed with some success for fine gravel beaches by Obhrai et al. (2008) who included a sediment permeability term in SHINGLE. However, for coarser sediments, the model still under-predicts overwashing and breaching and when wave conditions are characterised by spectra with bi-modal wave periods, overwashing

* Corresponding author at: School of Marine Science and Engineering, University of Plymouth, UK. Tel.: +44 23 80711840.
E-mail addresses: jwilliams@abpmer.co.uk (J.J. Williams), aruizdealegriaa@ii.unam.mx (A.R. de Alegría-Arzaburu), robert.mccall@plymouth.ac.uk (R.T. McCall), ap.vandongeren@deltares.nl (A. Van Dongeren).
[1] Tel.: +44 1752 584719.
[2] Tel.: +31 88 335 8273.

0378-3839/$ – see front matter © 2011 Elsevier B.V. All rights reserved.
doi:10.1016/j.coastaleng.2011.12.010

or crest erosion can greatly exceed the values suggested by parametric models (cf. Bradbury et al., 2011).

Further progress has been made with the beach profile model OTTP-1D (one-dimensional swash zone model with a porous layer). In this model an enhanced morphological capability has been implemented for gravel (Clark and Damgaard, 2002; Clark et al., 2004) and work by Lawrence et al. (2002) has coupled a 1D phase resolving Boussinesq wave model with sediment transport and morphodynamic modules for gravel with some success (e.g. Pedrozo-Acuna et al., 2007). However, validation of these models has been limited thus far by the availability of suitable data sets from the field and the laboratory (e.g. field measurements by Lorang, 2002; Bradbury et al., 2005; and laboratory studies by López de San Roman-Blanco et al., 2006; Obhrai et al., 2008).

To address some of the modelling deficiencies identified above, Roelvink et al. (2010) have developed XBeach,[3] a new open-source, process-based and time-dependent 2DH model of the nearshore and coast. This model solves coupled equations for cross-shore and longshore hydrodynamics and morphodynamics, including the generation of infragravity waves, and accounts for variation in hydrodynamic forcing and morphological development in the longshore dimension. The hydrodynamics and morphodynamics of XBeach have been extensively validated against (1D) flume experiments and some (2DH) field cases (Roelvink et al., 2009). In particular, the model showed qualitative skill in simulating dune erosion and overwash in measured cross-shore profiles of Assateague Island, Maryland (Roelvink et al., 2010) and good quantitative skill in measured topography at Santa Rosa Island, Florida, after Hurricane Ivan (McCall et al., 2010).

Our decision to use the XBeach model is motivated in part by the fact that most existing models for gravel beaches and barriers are parametric and fail to simulate hydrodynamic and sediment processes (e.g. wave transformations, run-up, sediment transport etc.). Further, existing numerical modelling approaches all have a range of deficiencies when considering coarse sediments and steep beaches. Although XBeach in its original form has been developed principally for sandy barrier environments, there are no obstacles to its application for gravel-sized material. However, swash asymmetry due to infiltration is an important physical process on gravel beaches and until recently has not been represented well in XBeach. To address this problem an XBeach variant has been developed by Jamal et al. (2010) that accounts for swash velocity asymmetry using: 1) a Lagrangian interpretation of velocity in place of Eulerian for driving sediment movement; 2) Packwood's (1983) model of infiltration; and 3) a new morphological module based upon Soulsby's (1997) sediment transport equation for waves and currents. Comparisons between laboratory results for gravel beaches presented by Pedrozo-Acuña et al. (2006) and predictions obtained using the modified XBeach model agree reasonably well. Although the predicted results are shown to compare well with the selected experimental data, the model has not yet been tested with varying mean water levels and for the real-world situations posing the greatest threat to life, property and the environment when gravel barriers and beaches are subjected to destructive overwashing.

In this paper we also account for swash asymmetry and infiltration, albeit in a different manner to Jamal et al. (2010), and use XBeach to simulate erosion and overwash measured in the BARDEX experiments (Williams et al., this issue). We also use XBeach to simulate the measured morphological changes on a natural gravel beach during a moderate storm lasting approximately 70 h. The paper first describes briefly the hydrodynamic and sediment components of the XBeach model. It then present results from a contrasting range of BARDEX tests and from the field site where the measured waves and tides are used to force the XBeach model, and comparisons are made between measured and modelled gravel barrier profiles. Attention is then focussed on the present ability of XBeach to contribute to the practical engineering requirement concerned with predicting threshold wave and water level conditions for gravel barrier overwashing.

2. XBeach model description

In the 2DH (depth-averaged) XBeach model, the most important hydrodynamic and sediment processes are modelled and coupled on the time-scale of wave groups (cf. Van Dongeren et al., 2003). The linkages between the primary modelling components are shown in Fig. 1a. In Fig. 1b the short and long wave components in XBeach are defined and are shown schematically. In XBeach, short (wind and swell) wave transformations are achieved using a wave action balance (e.g. Holthuijsen et al., 1989), and a roller energy balance is used to parameterise complex wave break processes in shallow water (e.g. Nairn et al., 1990; Stive and Dingemans, 1984). Wave forces accelerate or decelerate the flow described by the nonlinear shallow water equations (NSWE) and account is taken of long wave motions. Using the wave group varying mass flux associated with the short waves and rollers (e.g. Phillips, 1977), the Generalized Lagrangian Mean (GLM) approach (e.g. Walstra et al., 2000) is used to obtain Eulerian flow velocities thereby allowing inclusion of the mass flux contribution to the long wave motion and undertow. The equilibrium sediment concentration is obtained using computed hydrodynamic conditions and acts as a source term for the advection–diffusion equation for sediment (e.g. Galapatti, 1983). Bedload and suspended load sediment transport rates are computed

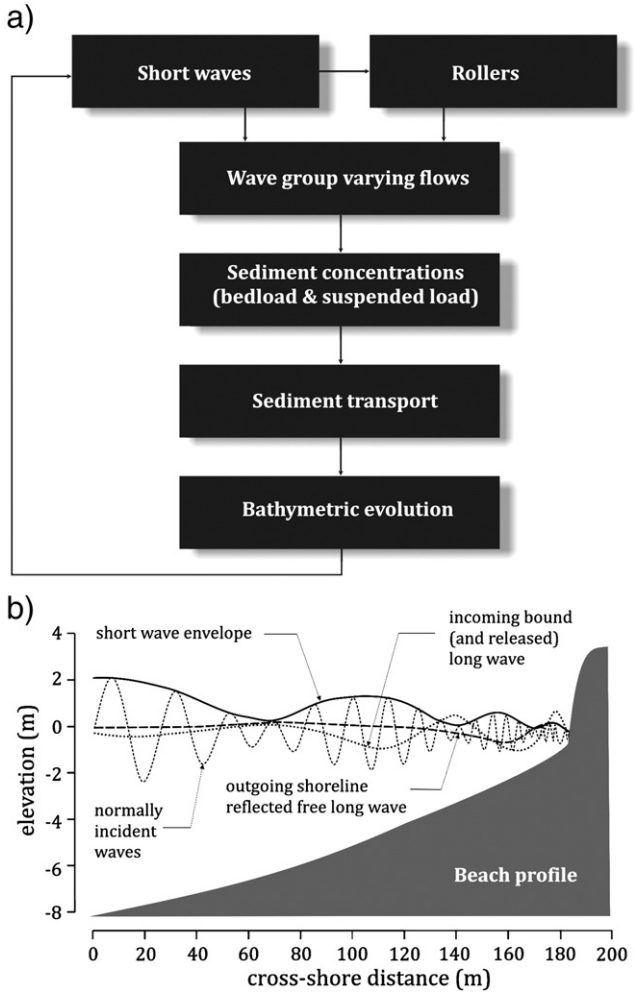

Fig. 1. a) Links between the primary modelling components of XBeach. b) Schematic representation of the short and long wave components in XBeach.

[3] http://oss.deltares.nl/web/xbeach/.

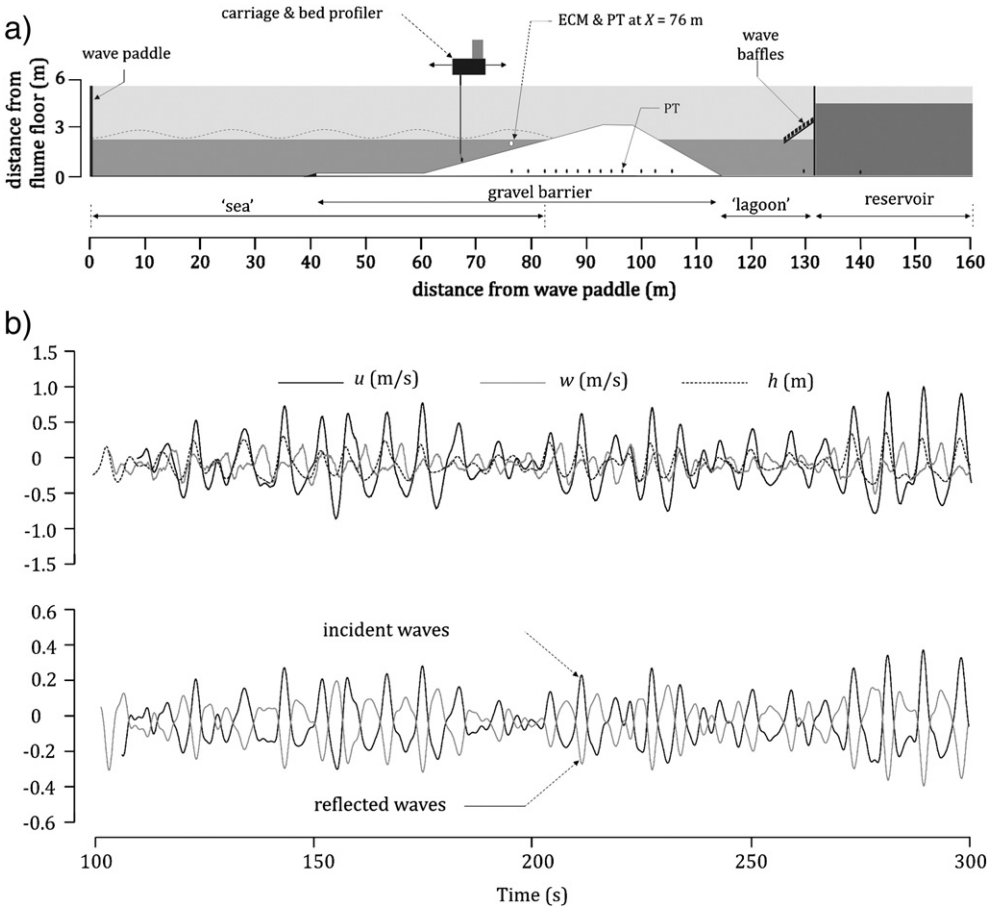

Fig. 2. a) Component parts of a typical BARDEX experiment. b) instantaneous, zero-mean time-series of wave-induced horizontal (u) and vertical (w) components and wave-modulated water depth (h) [upper panel] and typical incident wave time-series (and reflected waves) derived using the co-located gauge method [lower panel].

using the Van Rijn (2007) formulae. These are considered to be applicable for gravel-sized sediments in the present study. Bed level changes are computed from sediment transport gradients and take account of avalanching when slope gradients exceed pre-defined thresholds. XBeach accounts for feedback between the evolving bathymetry and the hydrodynamics at each time step. Recently XBeach has been extended by Van Thiel de Vries (2009) with an adapted wave dissipation model, an equilibrium sediment concentration formulation that depends on the bore averaged turbulence energy, and a wave shape model from which the bore interval is estimated. The wave shape model is also used to estimate intra-wave sediment transport and the dissipation rate in bores that develop after wave breaking.

On gravel beaches, bedload and sheet sediment flow are predominant. However, sediment transport equations applicable to gravel-sized sediments are scarce, largely empirical and are not well-tested in field or laboratory situations (e.g. Chadwick, 1989; Kleinhans and Van Rijn, 2002; Lawrence et al., 2001; Soulsby and Damgaard, 2005; Van Wellen et al., 2000). In the present study, the equilibrium sediment concentration, C_{eq} (Roelvink et al., 2009), is calculated using the extended transport formulation, ETF, of Van Rijn (2007). This method is built into XBeach and is considered to be suitable for the sediments used in the BARDEX experiments and for those at the field study site. In the ETF, sediment is mobilised in water depth h by the Eulerian flow velocity, u^E, and the near-bed short wave orbital motion, $u_{rms,2}$, in the form

$$C_{eq} = \frac{A_{sb}}{h}\left(\sqrt{(u^E)^2 + 0.64u_{rms,2}^2} - u_{crit}\right)^{1.5} + \frac{A_{ss}}{h}\left(\sqrt{(u^E)^2 + 0.64u_{rms,2}^2} - u_{crit}\right)^{2.4} \quad (1)$$

where A_{sb} and A_{ss} are bedload and suspended sediment transport coefficients, respectively, and u_{crit} is the threshold sediment entrainment velocity (see below). Following Reniers et al. (2004), $u_{rms,2}$ also includes the effect of wave breaking-induced turbulence so that

$$u_{rms,2} = \sqrt{u_{rms}^2} + 1.45k_b \quad (2)$$

where k_b is the bore-averaged near-bed turbulence (Van Thiel de Vries, 2009), and the peak wave orbital velocity is obtained from the wave group varying wave energy using

$$u_{rms} = \left(\frac{\pi H_{rms}}{\sqrt{2}T_m \sinh(k_w h)}\right) \quad (3)$$

where T_m is the mean intrinsic wave period and k_w is the wavenumber. The critical transport velocity for currents $u_{crit,c}$ is based on the Shields

Table 1
BARDEX test conditions examined in XBeach simulations.

Test	h_S (m)	h_L (m)	H_s (m)	T_p (s)
D2	1.75–3.25–1.75	1.50	0.8	4.5
D3	1.75–3.25–1.75	3.50	0.8	4.5
E8	2.50–3.63	3.50	1.0	8.0
E10	3.75	3.75	0.8	8.0

curve (cf. Van Rijn, 1993) and the critical flow for waves $u_{crit,w}$ is obtained using Komar and Miller (1975) so that

$$u_{cr} = \alpha u_{cr,c} + (1-\alpha)u_{cr,w,} \quad \text{where} \quad \alpha = \frac{u^E}{\left(u^E + u_{rms,2}\right)}. \tag{4}$$

In XBeach, changes in bed level, z_b, are computed using gradients of sediment transport rate which are assumed to occur on a timescale that is much longer than that associated with the hydrodynamic processes. In the 1D form of XBeach this is expressed as

$$\frac{\partial z_b}{\partial t} = \frac{1}{(1-p)}\left(\frac{\partial Sed_x}{\partial x}\right) \tag{5}$$

where p is the sediment porosity and Sed_x is the computed sediment transports in direction x:

$$Sed_x = hC\left(u^E + u_A \sin\theta_m\right)\frac{\partial}{\partial x}\left(D_h h \frac{\partial C}{\partial x}\right); \text{and} \tag{6}$$

where C is the actual depth averaged sediment concentration, θ_w is the mean wave angle, u_A mean flow component due to nonlinear waves, and D_h is a sediment diffusion coefficient $= \gamma_{visc}\nu_h$ (Van Thiel de Vries, 2009) where γ_{visc} is a calibration factor (≈ 1) and ν_h is the horizontal viscosity. XBeach also implements an algorithm to simulate avalanching if the bed slope exceeds a user-set critical value for wet or dry points in the model domain.

One of the critical features distinguishing a gravel beach from a sandy beach is the much greater permeability. This causes rapid infiltration of water during swash uprush, and much weaker backwash flows and gives rise to the widely reported asymmetry in swash velocity. To account for this, a refinement to the XBeach model used in the present study is the inclusion of a groundwater model computed according to the Darcy law in the form

$$Q = \frac{-\kappa A}{\mu}\frac{P}{L} \tag{7}$$

where the total discharge is Q, κ is beach permeability, A is the cross-sectional area to the flow, μ is the dynamic viscosity and P is the pressure drop over distance L. In XBeach this head gradient is found numerically. The use of the Darcy equation to model groundwater flows in gravel beaches is supported by strong evidence presented by Turner and Masselink (this issue). Further details of the exfiltration and infiltration algorithms used in XBeach are given by Roelvink et al. (2010). The 1D XBeach model equations used in the tests reported here are listed in Appendix A. Further details of XBeach are given by Roelvink et al. (2010) and Van Thiel de Vries (2009).

Owing to its widespread use in assessing the skill of coastal morphological models (e.g. Davidson et al., 2010; Pedrozo-Acuña et al., 2006;

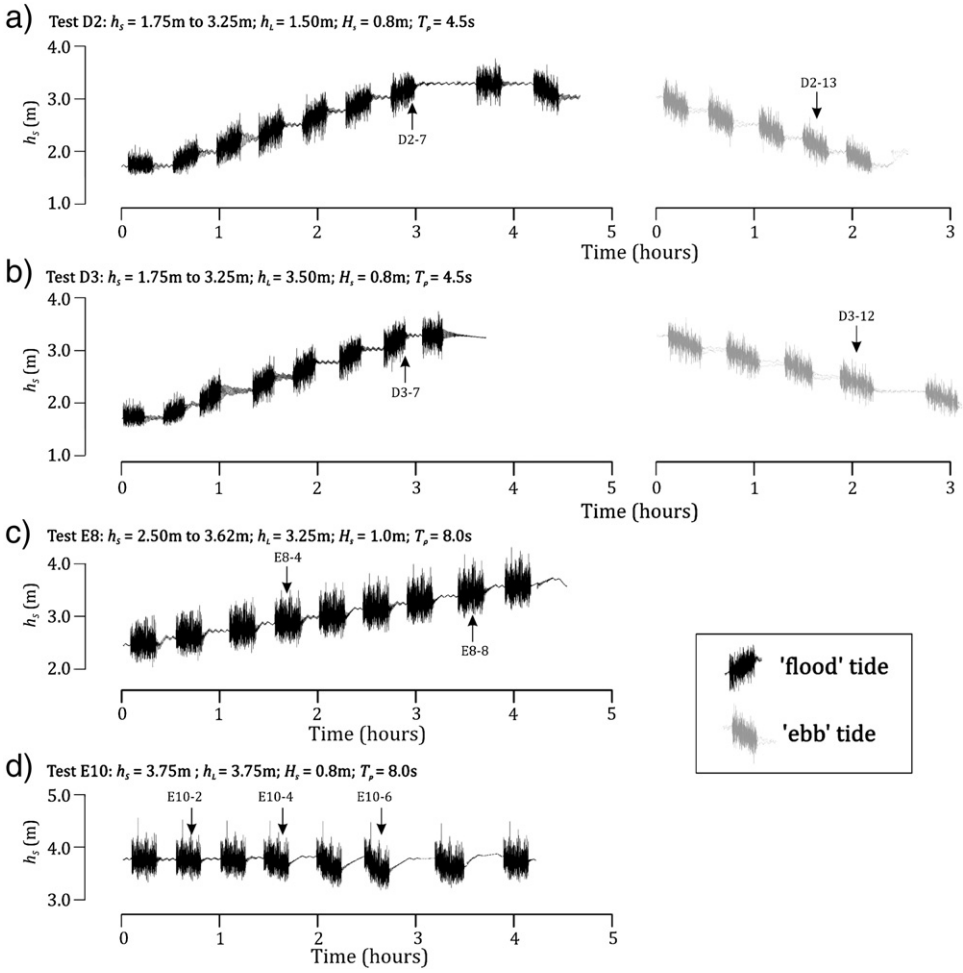

Fig. 3. The mean water level, h_S, and the combined water level and wave time-series used to run XBeach for BARDEX tests D2, D3, E8 and E10.

Sutherland et al., 2004) the 'skill' of a numerical model can be quantified using the Brier Skill Scores (BSS) statistical descriptor defined as

$$\mathrm{BSS} = 1 - \left[\frac{\left\langle (x_x - x_m)^2 \right\rangle}{\left\langle (x_b - x_m)^2 \right\rangle}\right]. \quad (8)$$

In the discussions below BSS values are used to quantify the agreements between observed beach profiles and beach profiles simulated by XBeach. Here x_b is the initial beach profile (baseline), x_m is the measured beach profile after the storm, and x_x is the beach profile predicted by XBeach. BSS values are used to define poor, moderate, good and excellent agreement between model predictions and observations (Van Rijn et al., 2003).

3. XBeach simulations of BARDEX experiments

Fig. 2a illustrates the components of a typical BARDEX experiment (see Williams et al., this issue) and defines a number of terms used in the sections below. These include: a) the gravel barrier; b) a water body termed 'sea' with a depth h_S, occupying a region of length approximately 82 m from the wave paddle to the barrier; and c) a water body termed 'lagoon' with a depth h_L, occupying a region of length approximately 25 m between the barrier and the water reservoir behind a gate in the flume at approximately 130 m from the wave paddle. In the BARDEX test, the 1D supra-tidal and sub-tidal barrier profiles were defined using measurements obtained using a roller and actuator, mounted on an overhead carriage (Fig. 2a, Williams et al., this issue), and *in situ* samples were used to determine a range of sediment properties required by XBeach. The measured values used were $D_{50} = 0.011$ m, $D_{90} = 0.0159$ m, $\rho_s = 2630$ kg/m^3, $p = 0.32$ and hydraulic conductivity, $K = 0.16$ m/s (Turner and Masselink, this issue). In order to optimise model run time and accuracy, the horizontal resolution of the XBeach model grid was set to 1 m. The initial groundwater profile was defined by quadratic interpolation between mean water levels measured by PTs on the seaward ($X = 76$ m) and lagoon ($X = 125$ m) sides of the barrier at the start of a given test sequence. Changes in mean water level during tidal simulation tests were measured by the seaward PT at $X = 76$ m and defined the 'tidal' input into XBeach. The incident wave time-series were derived using the co-located gauge method (Guza et al., 1984; Hughes, 1993; Kubota et al., 1990; Tatavarti et al., 1988; Walton, 1992) from a pressure transducer (PT) and a 40 mm-diameter electromagnetic current metre (ECM) at $X = 76$ m (Fig. 2a). These instruments measured water depth and the stream-wise and vertical wave-induced flows, respectively. PT and ECM data were smoothed using a digital 5-point forwards–backwards filter and the PT data were corrected for frequency-dependent depth attenuation. The upper panel in Fig. 2b shows instantaneous, zero-mean time-series of wave-induced horizontal (u) and vertical (w) components and wave-modulated water depth (h). The lower panel in Fig. 2b shows typical incident wave time-series (and reflected waves) derived using the co-located gauge method.

In BARDEX tests, waves were used to drive the XBeach model using two approaches. In *Case A* the model domains in the x and z directions were $50\ \mathrm{m} < X < 125$ m and $0 < z < 5$ m, respectively, with a horizontal resolution of 0.5 m. Tests showed that the use of higher resolution model grids added greatly to the model run time and had little effect on XBeach predictions. The "offshore" boundary was located close to the BARDEX beach and measured incident waves were imposed at this boundary. This allowed short waves to be input using the standard non-linear shallow water equations (cf. Peregrine, 1972). An absorbing-generating boundary condition developed by Van Dongeren and Svendsen (1997) allows long waves to propagate freely out of the model on the offshore and lagoon boundaries with minimal reflection. Wall boundary conditions were applied for the flow and sediment transport on the lateral (shore-normal) boundaries.

Although this approach is useful when measured incident wave time-series are available, it is very unlikely that such data will be available for field sites. In these circumstances the simulation of future storm impacts must rely on less well-defined wave conditions at the offshore boundary of the model. However, this uncertainly can be accommodated in XBeach through the use of wave spectra in a range of common formats. Therefore before using XBeach to predict the storm impact at our selected field location where only wave spectra are available to define offshore wave conditions, we first evaluate model performance using measured wave spectra as the wave forcing in a second series of tests for a range of BARDEX experiments. In *Case B*, we keep the same model setup as *Case A* and input waves as JONSWAP spectra at the location of the wave generator in the Delta flume. Parameters defining the spectral estimate of significant wave height, *Hm0*, peak wave period, *Tp*, and mean wave direction, θ_w, were determined using the incident wave time-series measured at $X = 76$ m. The peakedness factor, γ_j, and spreading function, n_s, were defined as 3.3 and 2, respectively. This approach allowed direct comparison between XBeach model results in the laboratory experiments with results from the field test case where only wave spectra were available to drive the XBeach model.

The BARDEX experiments selected here to demonstrate typical results from the XBeach model include: a) tests D2 and D3, with high and low lagoon levels, a complete tidal cycle and moderate waves; b) test E8, with a high lagoon level, rising tide and large waves; and

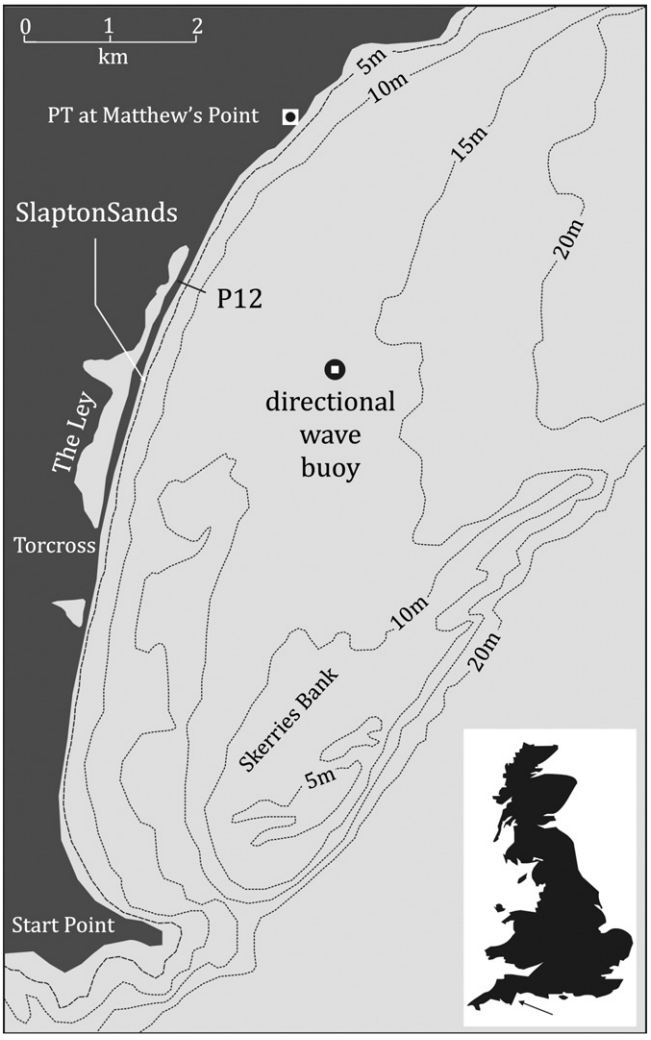

Fig. 4. Map of Slapton Sands, SW UK showing the location of the barrier test profile P12, the directional wave buoy and the PT at Matthew's Point.

c) test E10 with high lagoon and sea level and large waves (for overwash). These test conditions are summarised in Table 1. The mean water level, h_S, and the combined water level and wave time-series used to run XBeach for each of the tests are shown in Fig. 3. In Fig. 3a and 3b, the time-series are split into rising and falling limbs to distinguish simulated 'flood' and 'ebb' tides, respectively. Individual 'runs' in a given test are identified using arrows. The beach profiles used to define the initial topography and bathymetry in the XBeach model at each tidal step in a given tidal sequence (Fig. 3) were defined in two ways: a) using the measured profile at the end of the previous test; and b) using the profile predicted by XBeach at the end of a given test in the sequence. These two approaches are referred to below as '*reset*' and '*no-reset*' tests. This approach had two objectives: a) *reset* tests aimed to examine short-term XBeach performance over a range of tidal and lagoon levels and prevented model prediction errors from influencing subsequent tests in a sequence; and b) *no reset* tests aimed to include all prediction errors from the model as the simulation progresses through the test sequence. This allowed examination of longer-term model performance and the cumulative effect of prediction errors.

4. XBeach simulations of storm conditions and overwash at Slapton Sands

Although XBeach simulations of BARDEX tests allow a good assessment of model performance at the laboratory scale, it is also considered important here to assess the performance of the model at the full field-scale, and over an extended period during a storm. Doing so allows an objective assessment of XBeach in its present state of development and an appraisal of its utility as a predictive tool for some practical engineering and coastal management purposes. To do this we have elected to use field measurements obtained on a natural gravel beach and to make comparisons between observed changes in beach morphology with XBeach predictions of beach profile responses to a real storm.

The field site chosen for the study is located at Slapton Sands, a steep (average $\tan\beta = 0.12$), 4.5 km-long and 100 m to 140 m-wide macrotidal gravel barrier (average $D_{50} = 6$ mm, $\rho_s = 2500$ kg/m^3) between two cliff outcrops in Start Bay, southwest England, (Fig. 4). A beach profile located at the northern end of The Ley (P12, Fig. 4) is selected as the test case. XBeach is used to model the response of this profile to an easterly storm that began during spring tides on 17

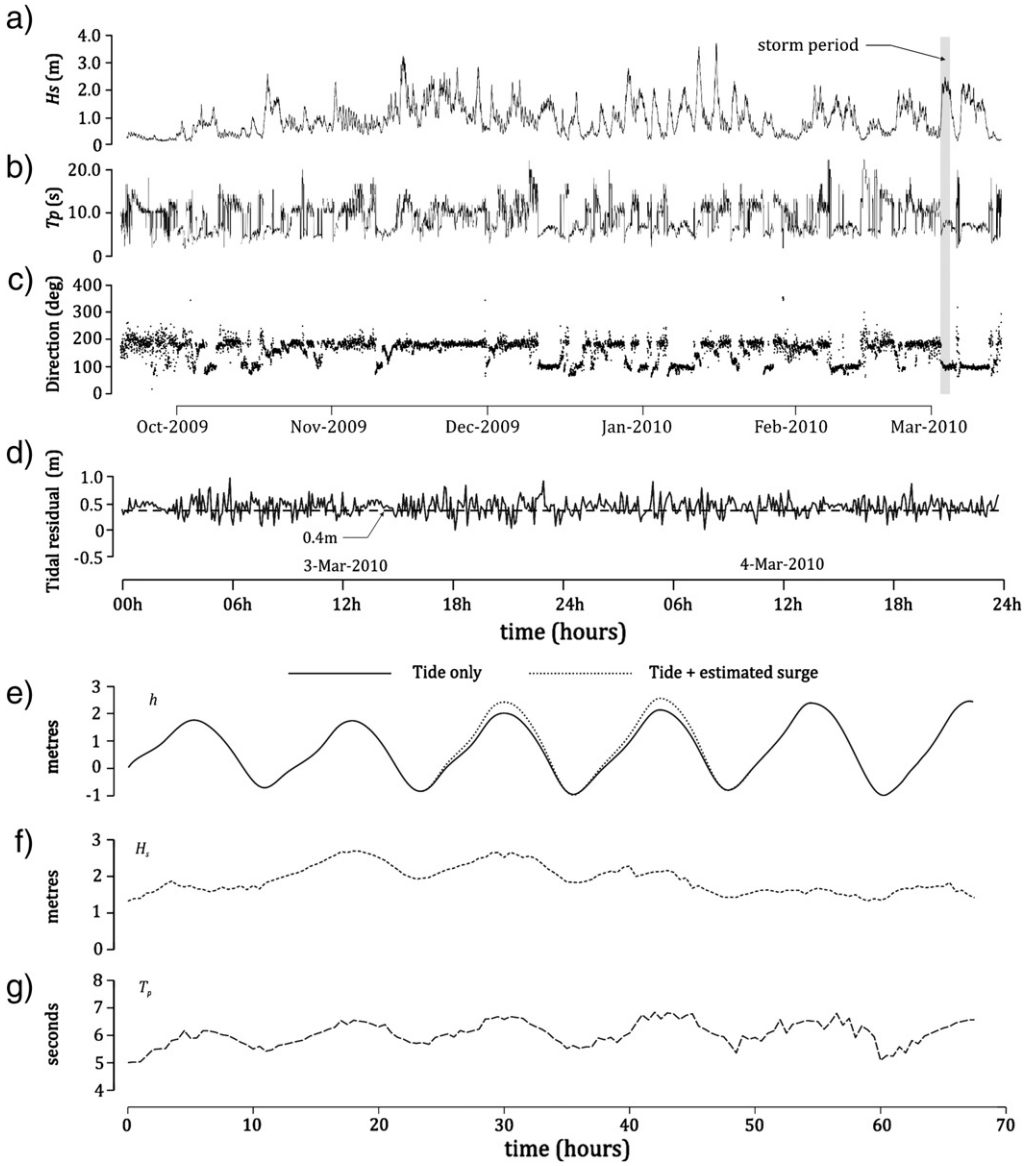

Fig. 5. a) to c) Wave data for the period October 2009 to March 2010. d) Tidal residuals for the period 3rd March to 4th March, 2010, e) tide and tide plus surge time-series used in XBeach storm simulation for Slapton profile P12. (f and g) Significant wave height and peak wave period time-series used in XBeach storm simulation for Slapton profile P12.

April 2008 and lasted for approximately 70 h causing erosion of the supra-tidal beach profile. Wave data from a directional wave buoy located approximately 2 km offshore from Slapton Sands in approximately 10 m ODN[4] (Fig. 4) showed that during this time H_s exceeded 2.5 m and T_p was approximately 7 s.

Although the beach profile was measured using RTK-GPS well before the storm on the 7th April 2008, calm waves (H_s<0.3 m) predominated during the period from 7th to the 17th April, and thus this beach profile is considered to approximate closely the pre-storm condition and is used to define the pre-storm topography and bathymetry in the model. A second beach survey obtained at the end of the storm on 19th of April 2008 is used to define the post-storm beach profile. It was not possible to obtain profile measurements at more than 1.5 m below the low water line and it was necessary to infer the initial offshore profile by taking the measured sub-tidal beach slope at $z=-1.5$ m ODN and extrapolating to $z=-5$ m ODN. The water depth in a region extending a further 50 m offshore was then set to −5 m ODN. To enable the investigation of beach overwashing thresholds, and to allow inclusion of a realistic beach groundwater profile in XBeach, the beach profile was extended to the lagoon. The initial groundwater profile used in the model was idealised to represent the normal situation at Slapton Sands with the lagoon level approximately 2.5 m above ODN (Austin and Masselink, 2005). In all XBeach simulations of Slapton Sands, the model domains in the horizontal and vertical directions were 0 m<x<200 m and −5 m<z<6 m, respectively, with horizontal and vertical resolutions of 1.0 m and 0.5 m, respectively.

Tidal levels during the storm examined in the XBeach model were estimated using a validated tidal model. This was developed for Slapton Sands using Fourier analysis of existing pressure sensor data to obtain tidal constituents. However, a lack of tidal measurements at Slapton during the storm considered here prevented estimation of the residual surge component, h_{surge}, known to be particular significant during easterly storms. Data from the directional wave buoy and from a pressure sensor deployed at Matthew's Point (Fig. 4) during the period October 2009 to March 2010 were used to find recent easterly storm events with H_s O(2.5 m) and T_p O(7 s). These wave data are shown in Fig. 5a, b,c and a grey shaded area, spanning the period for 3rd to 4th March 2010, denotes the easterly storm most similar to the one examined here. The tidal residuals for this storm are shown in the lower panel of Fig. 5d. These were obtained from the tidal record and de-trended to remove wave effects using a Fourier fitting technique.

Owing to uncertainty in the actual h_{surge} value for the April 2008 storm, moderate h_{surge} values of 0.4 m were added to the peak tidal elevations using a smoothing function. Fig. 5e shows the predicted tidal time-series and the estimated surge component used in the XBeach model of the Slapton profile P12. Spectral wave data recorded at half-hourly intervals by the directional wave buoy (Fig. 5f,g) were transformed using the Mike21 SW flexible mesh spectral wave model and used to define the wave spectra at the offshore boundary in the XBeach model ($z=-5$ m). D_{50}, D_{90} and ρ_s values were measured at P12 (0.006 m, 0.009 m and 2500 kg/m^3, respectively). Changes in mean tidal level and wave spectra were input into the model in a series of steps, each lasting 1800 s. During execution, XBeach uses interpolation to produce a seamless change between varying tidal and wave conditions. The value of z_0 in the sediment transport formulae was set to the recommended value of 0.006 m (Soulsby, 1997). As other parameter settings in XBeach have thus far remained untested for gravel beaches, we start by using the recommended settings for sandy beaches in the knowledge that the majority of these only affect hydrodynamic behaviour and are largely unaffected by the composition of the bed sediments. However, two parameters have been found to influence the model predictions. These are the friction factor (or drag coefficient), normally set to 0.002 for sand-sized sediments in XBeach (cf. Soulsby, 1997) and the hydraulic conductivity, K. The value, role and influence of these parameters in the present application of XBeach for gravel-size sediments are discussed below. The groundwater module in XBeach was invoked in all model runs.

[4] Ordnance Datum Newlyn.

5. Results and discussion

In the presentation and discussion of results from the BARDEX tests and from Slapton Sands we make the assumption that good agreement between measured and predicted beach profiles indicated by BSS values, demonstrates that the parameter settings used in XBeach are appropriate for each test case considered. In general these have been selected following the guidelines in the XBeach manual (Roelvink et al., 2010) and are listed in Table 2.

5.1. BARDEX test cases

5.1.1. Case A: forcing XBeach with short waves

Measured and predicted gravel barrier profiles from the XBeach model driven by short waves at the end of the runs indicated by

Table 2
Typical XBeach parameter settings for BARDEX and Slapton tests.

Parameter	Setting	Parameter	Setting
Grid input		nuhfac	0.8
nx	100	nuhv	5
ny	2	turb	2
xori	0	***Limiters***	
yori	0	gammax	5
alfa	0	hmin	0.01
vardx	1	eps	0.01
depfile	bathy.txt	umin	0.01
xfile	X.grd	hwci	0.01
yfile	Y3.grd	scheme	2
posdwn	−1	carspan	0
Waves		***Boundaries***	
thetamin	−80	front	1
thetamax	80	back	2
dtheta	10	left	1
instat	3	right	1
taper	0	***Sediments***	
order	2	z0	0.006
ARC	1	form	2
dir0	270	dico	5
rt	1200	tsfac	0.1
dtbc	0.2	D50	0.011
break	3	D90	0.016
wci	1	rhos	2530
wcits	1	thetanum	0.5
roller	1	Tsmin	0.01
beta	0.2	tfac	0.1
gamma	0.9	tsfac	0.1
alpha	0.5	CFL	0.7
delta	0	***Morphology***	
n	10	morfac	1
swtable	RFTable.txt	morstart	0
dzsdx_cr	0.1	por	0.4
facthr	7.5	dryslp	1
Tide		wetslp	1
tideloc	2	hswitch	0.01
zs0file	tide.txt	facua	0.5
tidelen	2	facsl	1.6
paulrevere	0	***Time steps***	
Groundwater		tstop	914.4
gwflow	1	tstart	0
kx	0.05	tintg	0.2
kz	0.05	tintp	0.2
dwetlayer	0.2	***Output***	
aquiferbot	0	nglobalvar	4
gw0file	gw0.dat	zb	–
Flow		zs	–
cf	0.007	gwhead	–
nuh	0.5	Subg	–

arrows in Fig. 3 are shown in Fig. 6a for BARDEX experiments D2, D3 and E8. Panels on the left show results obtained approximately mid-way through a stated BARDEX test and those on the right show results at the end of the same test. All the figures show the mean water level measured by the PTs and predicted by XBeach, the measured beach profile before and after a test run over the range of 70 m$<X<$110 m, and the predicted barrier profile for *reset* and *no reset* model runs. Looking at the *reset* results first, Fig. 6a shows that although XBeach predicts beach erosion losses at approximately the correct location, the losses are larger in magnitude than the measured values. Similarly, the zone of accretion, seaward of the erosion region, predicted that accretion exceeds the observed values. Although the *no reset* test results are similar to the *reset* tests with regard to the location of erosion and accretion zones, the amount of erosion and accretion is larger in all *no reset* cases. As expected this shows that XBeach errors in the early stages of a test run influence subsequent beach profile development. In all cases, good agreement between the measured and predicted mean water levels is demonstrated indicating that the groundwater module in XBeach is functioning accurately.

5.1.2. Case B: forcing XBeach with long waves

Measured and predicted gravel barrier profiles from the XBeach model (no reset) using long wave forcing are shown in Fig. 6b for runs D2-13, D3-12 and E8-8 at the end of a given test sequence. Also shown are the results from the XBeach model (no reset) using short wave forcing. In these cases measured and predicted mean water level are identical to that shown in Fig. 6a and are not illustrated again here. Although Fig. 6b shows that in these typical test results, the XBeach model results using short and long wave forcing are closely similar, in all test cases examined, XBeach tends to predict slightly more erosion for the long wave case (approximately 3% by volume). There is also a correspondingly larger accretion volume offshore that tends to be distributed along the profile in a manner closely similar to the short wave cases.

5.1.3. Predicted beach profile evolution

XBeach results for *Case A* experiments D2, D3 and E8 shown in Fig. 7 show temporal and spatial *differences* between predicted and measured beach profiles over the range of 50 m$<X<$100 m for *reset* and *no reset* tests. Tests D2 and D3 show the spatial translation of the erosion/accretion zone up and down the beach profile in response to the full tidal cycle forcing (Fig. 3). Test E8 only shows the active erosion/accretion zone moving up the beach profile in response to a rising tidal level (Fig. 3). For *reset* tests, the maximum differences between observed and predicted profiles are only 0.1 m for tests D2 and D2, and only 0.2 m for test E8. In all cases the locations of maximum discrepancy between measured and predicted profile values are associated with regions of accretion. For the *no reset* tests we observe quite different results. For tests D2 and D3, the over prediction of accretion at $X=c$. 60 m tends to increase through time as the tide rises to its maximum level and eroded sediment is added to this portion of the profile. At the same time, erosion further up the profile is larger

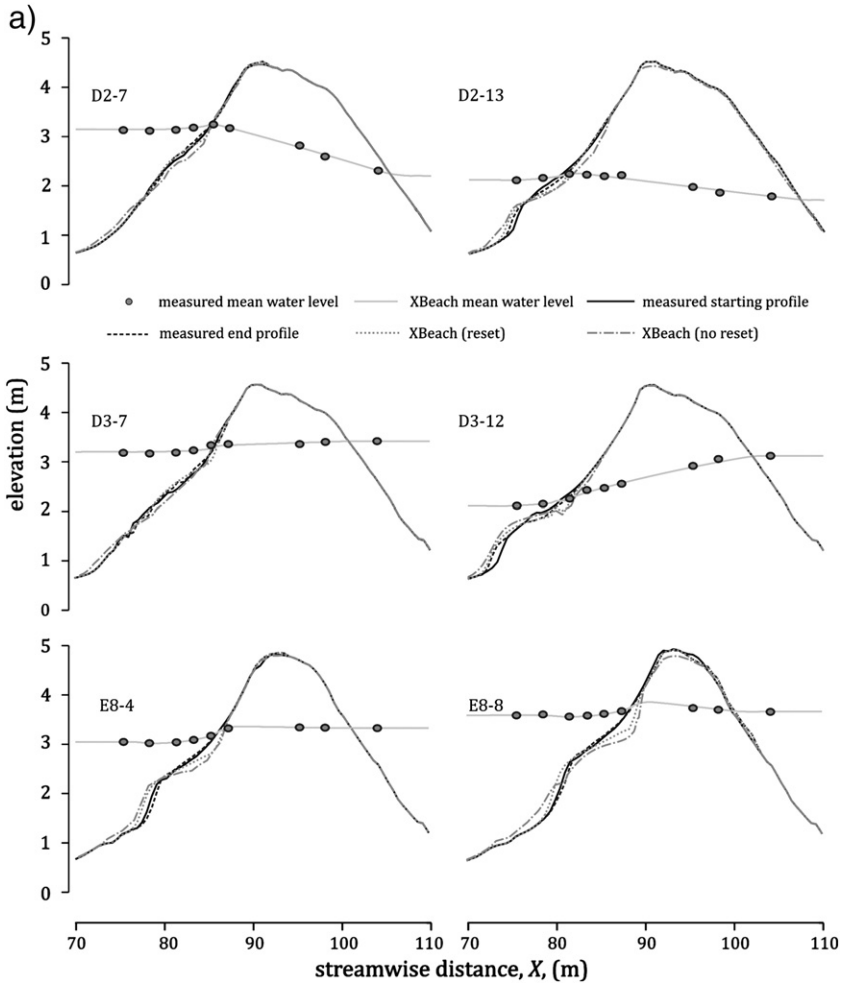

Fig. 6. XBeach results for BARDEX tests D2, D3 and E8. Panels on the left show results obtained approximately mid-way through a stated BARDEX test and those on the right show results at the end of the same test. All the figures show the mean water level profile predicted by XBeach, the measured beach profile before and after a test run over the range of 60 m$<X<$110 m, and the predicted barrier profile for *reset* and *no reset* model runs.

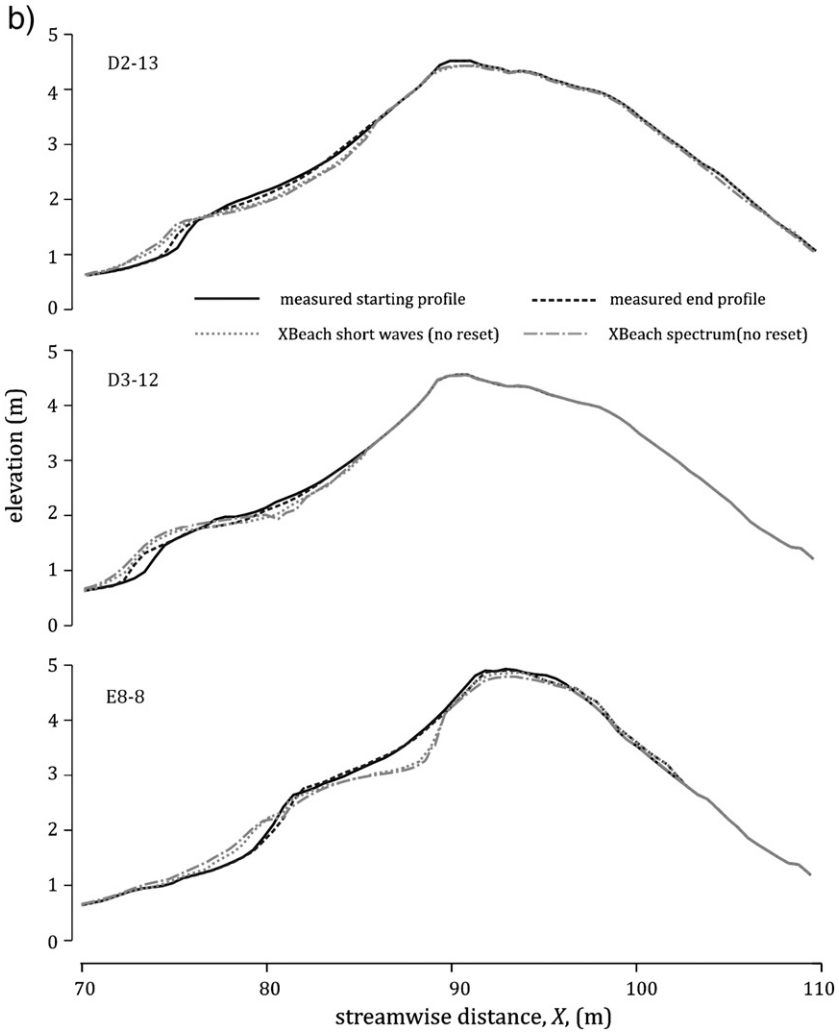

Fig. 6 (*continued*).

and results in beach lowering of approximately 0.2 m around the time of the maximum tidal level in the test. The same trends in predicted beach profile response are also observed for test E8. During the falling tide in tests D2 and D3, the eroded beach does not recover and further offshore accretion occurs. In these cases XBeach fails to replace all the eroded sediment as the tidal level falls.

Changes in measured and predicted beach volume per metre width were also examined to further assess XBeach performance. The beach profile was split into three regions: a) sub-tidal; b) inter-tidal; and c) supra-tidal. Fig. 8 shows the *Case A* results of this analysis and includes a definition of each tidal region. For tests D2 and D3, beach volume changes predicted in the sub-tidal region in *reset* tests are closely similar to the measured volumes. Not surprisingly, differences between predicted and measured beach profile evolution in the inter-tidal and supra-tidal regions through time are larger. For the *no reset* tests, differences between measured and predicted beach volumes in each tidal region are larger than the in the *reset* cases. Although also showing a tendency to increase through time, Fig. 8 shows evidence that the differences between measured and predicted profiles tend towards a constant value by the end of the test sequences thus indicating that the predicted profile has attained a form of equilibrium with the applied forcing conditions. We see similar result in the case of test E8. However, in this case, probably owing to the larger waves, the differences between measured and predicted beach volumes are larger.

5.1.4. Overwash

Results from the *Case A* overwash tests E10 are shown in Fig. 9 for runs 2, 4 and 6 (identified in Fig. 3). Fig. 9a shows that for run E10-2, erosion of the front face of the barrier, lowering of the barrier crest, and deposition of sediment on the lagoon-facing side of the barrier are well reproduced in the XBeach simulation. Similarly, Fig. 9b shows good agreement between the measured and simulated barrier profiles for overwash test E10-4. Together, these results provide compelling evidence that overwash sediment transport is accurately simulated in XBeach. In Fig. 9c, depicting results from overwash test E10-6, erosion of the seaward face of the barrier is reproduced with some skill. However, in the XBeach simulation the crest region is lowered by approximately 20 cm more than is measured and the resulting sediment is deposited on the lagoon-facing barrier slope, where further discrepancies between measured and predicted profiles are evident. It is also noted that in run E10-6 gravel 'mega-ripples' are present on the seaward-facing slope of the barrier at approximately 80 m$<X<$approximately 90 m in water-depths ranging between approximately 1.5 m and 2.5 m. These bedforms are shown in the inset photograph in Fig. 9c. These bedforms were present in the later series of BARDEX tests with large waves ($H_s = 1.0$ m, $T_p = 8$ s,) and XBeach always tended to smooth these features out.

Since in *Case A* tests XBeach is driven by incident wave time-series, it was possible to compare the temporal occurrence of predicted overwash events with overwash events measured using the instrument arrays deployed across the barrier (cf. Williams et al., this issue; Matias

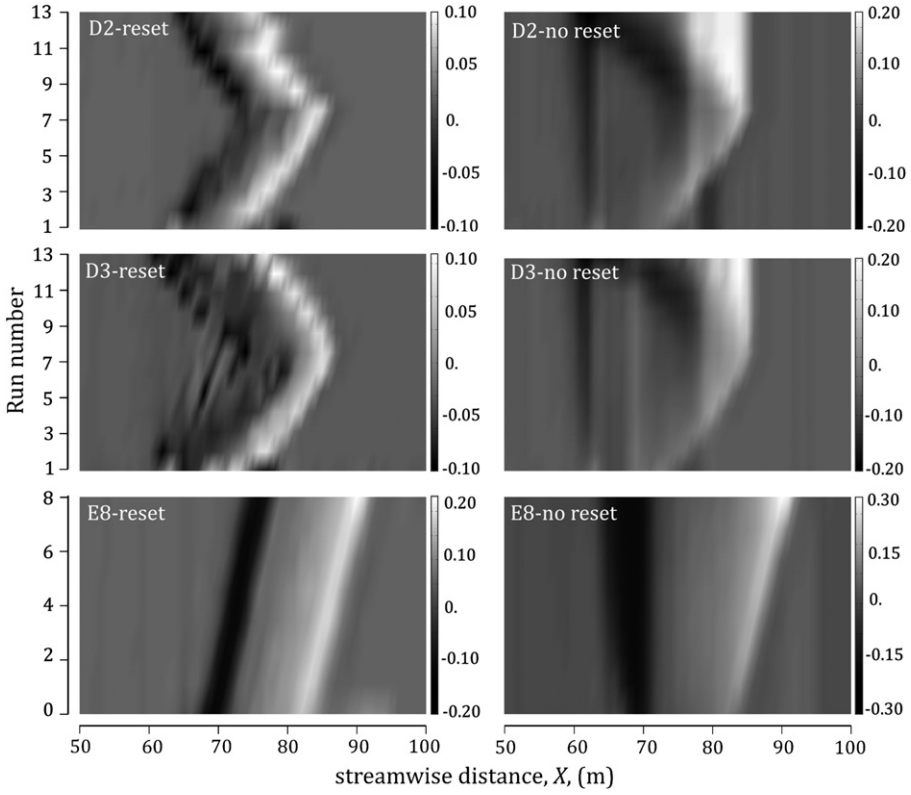

Fig. 7. Temporal and spatial differences between predicted and measured beach profiles over the range of 50 m<X<100 m for *reset* and *no reset* tests for BARDEX tests D2, D3 and E8.

et al., this issue). XBeach results for test series E10 demonstrated that the model was able to simulate accurately both the flow depth and flow velocity associated with most measured overwash events. XBeach also provided reliable information on threshold wave heights for the first observed overwash event in a test sequence. However, the threshold prediction was less reliable as test sequences proceeded owing to the overestimation of barrier crest lowering and an underestimation of berm formation by swash uprush events. Nevertheless XBeach demonstrated an ability to predict the threshold wave and mean water level conditions resulting in initial barrier overwash and accounted for changes in barrier morphology attributable to sediment transport by overwash flows.

BSS scores for the present XBeach model predictions at the end of each run in the *Case A* BARDEX test (i.e. short waves) are given in Table 3. Also shown are mean BSS ($\bar{X}$) and standard deviation BSS (σ_x) values for each test. These data show that for the majority of BARDEX tests considered here, BSS value exceeds a critical value of 0.45 which is judged to be '*reasonable/fair*' according to criteria established by van Rijn et al. (2003). In many other cases, BSS values exceed 0.6 and indicate 'good' agreement between measured and predicted profiles by the same criterion. Table 3 shows that BSS values for *no reset* tests were $O(10\%)$ lower than for the *reset* tests for the first runs in tests D2, D3, E8 and E10. For tests D2, D3 and E8, these differences increased to approximately 25% by the end of a run and to approximately 80% in the case of E10. BSS scores for the present XBeach model predictions at the end of each run in the *Case B* BARDEX test (i.e. long waves) are given in Table 4. In virtually all examples BSS values for *Case A* tests are slightly higher than for *Case B*. Further, these differences increase as a given BARDEX test proceeded so that differences between *Case A* and *Case B* BSS scores at the end of a given test were approximately twice the initial values. In spite of these differences, it is considered that XBeach model predictions are reasonably accurate irrespective of the wave forcing method.

5.2. Slapton Sands test case

Storms cause large shoreline variability at Slapton Sands (Ruiz de Alegria-Arzaburu et al., 2010b), and a combination of field measurements and ARGUS video observations have shown that this variability is highly dependent on the wave direction (Ruiz de Alegria-Arzaburu et al., 2010b). Although during easterly storms the beach profile adjusts primarily in the cross-shore direction, greater erosion frequently occurs at the northern end of the barrier, and the greatest alongshore sediment exchanges occur during southerly storms (Ruiz de Alegria-Arzaburu and Masselink, 2010a). However, as easterly storms are dominated by cross-shore sediment transport, the use here of a 1D version of XBeach is considered to be justified.

Measured beach profiles at P12 before and after the easterly storms described above are shown in Fig. 10a. This figure also shows end-of-storm profiles predicted by XBeach for a range of surge level enhancements to the tidal forcing from no enhancement to a maximum value of +0.4 m indicated by the PT data from Matthews Point for a storm with similar characteristics. This approach is justified here for two reasons: a) preliminary tests using only the astronomical tide resulted in a significant under-prediction of erosion at the correct location along the measured profile; and b) measured tidal levels during storms indicate strongly that a surge component $O(0.4)$m is associated with easterly storms with approximately the same characteristics as the one studied here. In common with the BARDEX results discussed above, there is a tendency in the XBeach predictions for significant accretion along the lower part of the beach profile. However, it is not possible to assess how realistic this is as no data for this part of the beach profile could be obtained. This uncertainty is indicated in Fig. 10a by the "?" symbol. Fig. 10a also shows that XBeach tends to over-predict erosion of the upper section of the profile irrespective of the surge level considered. The best agreement between measured and predicted profiles at the end

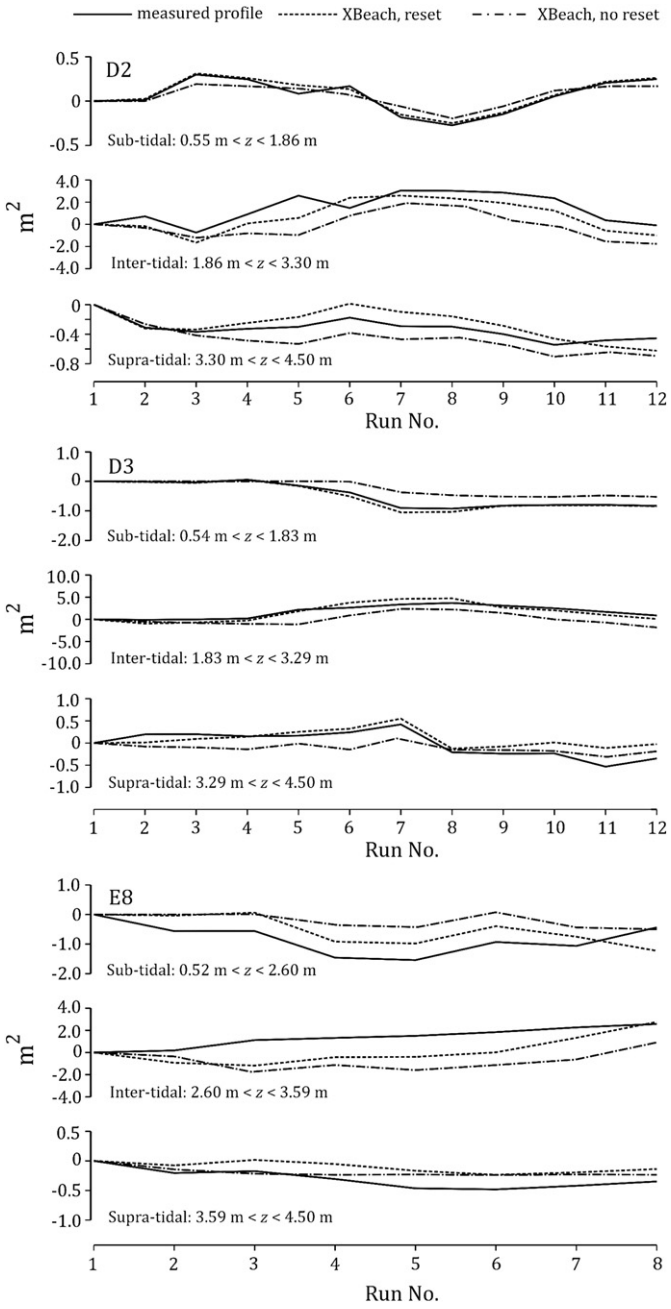

Fig. 8. Measured and predicted changes in beach volume per metre for sub-tidal, inter-tidal and supra-tidal regions for BARDEX tests D2, D3 and E8.

of the storm were obtained using a surge enhancement of 0.4 m (BSS = 0.66).

At Slapton Sands, the groundwater dynamics are normally characterised by a seaward directed groundwater flow (Austin et al., 2009). XBeach model results showed that when the lagoon water table (LWT) was <MHWS, the beach drained with greater efficiency and eroded less. Consequently the beach face remained steep. Austin and Masselink (2005) have previously attributed a reduction in sediment transport at mid-upper swash zone on gravel beaches to larger rates of infiltration, which by reducing sediment transport competency of backwash, tend to bias onshore sediment transport. When LWT > MHWS, supra-tidal erosion was greater and more inter-tidal accretion occurred resulting in flattening of the beach face. These results agree well with findings of Austin et al. (2009) for BARDEX experiments, and with Masselink et al. (2010) based on field data collected at Slapton Sands. XBeach results for Slapton are therefore consistent with previous findings and show that the decision to include the beach groundwater in XBeach simulations is well-justified.

It was noted above that the two XBeach parameters thought most likely to influence model performance for gravel beaches were K and C_f. As both were found in initial trials to influence beach profile development in the XBeach model, it was necessary to establish appropriate values. Setting K to 0.05 m/s, a value reported by Austin et al. (2009) for Slapton Sands, sensitivity analyses were undertaken for C_f. Fig. 10b shows that for $C_f = 0.005$, erosion on the upper beach and accretion on the lower beach are overestimated. Increasing C_f to 0.01 results in the opposite effect. A C_f value = 0.007 was found to give the highest BSS values for the measured and the predicted beach profile for the measured K value of 0.05 m/s. With a suitable C_f value now established, sensitivity analyses were then undertaken for K in the range of 0.01 m/s to 0.16 m/s. Results of these tests are shown in Fig. 10c. These show that for $K = 0.01$ m/s, erosion on the upper beach and accretion on the lower beach are overestimated. Increasing K to 0.16 m/s results in less accretion on the lower beach and an underestimation of erosion on the upper beach. The highest BSS value was obtained for $K = 0.05$ m/s.

Masselink and Li (2001) report that enhanced beach accretion in the swash zone only occurs when the total infiltration over a wave cycle exceeds approximately 2% of the total uprush volume. This can only occur when the hydraulic conductivity exceeds 0.01 m^{-1} and thus requires grains coarser than approximately 1.5 mm. Since D_{50} for BARDEX and Slapton are 11 mm and 6 mm, respectively, it would be expected that around 15% to 30% of the swash volume per wave cycle would infiltrate into the beach face, thus reducing sediment transport and influencing beach morphology (Austin and Masselink, 2005, 2006; Mason and Coates, 2001; Masselink and Li, 2001). The results support previous finding by Masselink and Li (2001) and Austin (2005) indicating that K is a factor controlling swash infiltration and this in turn influences beach morphology.

Fig. 11 shows temporal and spatial changes in the Slapton beach profile predicted by XBeach during the easterly storm period. It shows areas of erosion and accretion sweeping up and down the beach profile in response to the tidal variations in the mean water level and to the waves. At the start of the simulation, when the tidal level is low, a zone of erosion, attributable to wave action, yields material that is deposited in a zone extending approximately 10 m offshore from a weakly developed step feature similar to the feature observed in the field (cf. Austin and Buscombe, 2008). As the tidal level rises, the zone of erosion translates up the beach, and material previously deposited offshore is mobilised and swept up the beach, restoring the profile approximately to its configuration before erosion. On reaching the maximum tidal level, erosion of the upper beach extends a few metres and results in some scarping of the upper beach face. During the falling tide material deposited in the offshore accretion zone is remobilised and is moved progressively offshore in a zone between approximately 2 m and 3 m below the mean tidal level. As the tide again rises, the offshore material is once more swept back up the beach and replaces material eroded during the previous falling tide. Further beach scarping occurs during high water. After a few tidal cycles the beach profile adjusts to the applied tide and wave forcing, and subsequent changes in the profile are greatly reduced.

The second feature in this simulation concerns the erosion along the upper part of the profile in the cross-shore region between approximately 90 m and approximately 120 m. At the start of the simulation, Fig. 11 shows that erosion extends a cross-shore distance approximately 15 m from approximately 75 m to approximately 90 m. By $t + 40$ h, the eroded portion of the beach has extended a further 25 m to approximately 115 m and by $t + 70$ h, erosion reaches nearly 120 m. It is notable that the rate at which this erosion zone extends up the beach decreases approximately exponentially through time, indicating that the beach profile in the model is evolving towards a quasi-equilibrium state. Although peak tidal levels increase

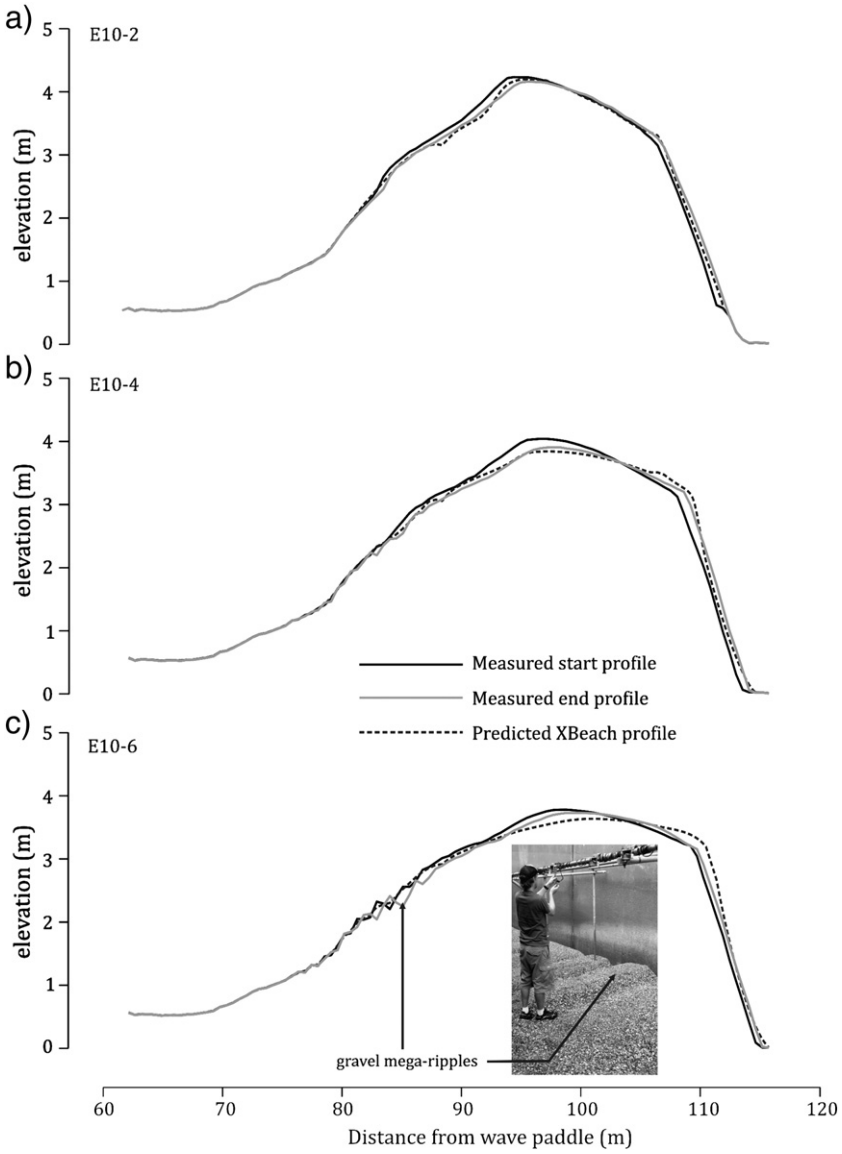

Fig. 9. Measured and predicted barrier profiles from overwash tests E10 for runs 2, 4 and 6 (identified in Fig. 3).

throughout this simulation, these results probably also reflect the decrease in H_s values during the storm period (Fig. 5f).

Although reference is made here to a step-like feature that moves up and down the beach profile with the rising and falling tide, the modelled feature is not strictly speaking the step reported by Austin and Buscombe (2008). This erosive feature is most likely the result of offshore sediment transport by the undertow. Given its position relative to the mean water level suggests the feature would be more accurately described as a breakpoint bar.

The temporal evolution of the beach profile in the XBeach simulation is further illustrated in Fig. 12 which shows changes in beach volume (assuming the profile is 1 m wide) for the supra-tidal (2 m to 6.2 m ODN), inter-tidal (−2 m to 2 m ODN) and sub-tidal (−5 m to −2 m ODN) sections of the profile. It shows a net balance between losses and gains, with erosion occurring primarily in the supra-tidal region, and accretion in the inter-tidal and sub-tidal regions. It shows also that erosion and accretion rates decrease through time as the profile tends towards a stable form with the prevailing hydrodynamics. The step-like nature of erosion and deposition is one frequently observed in the field on natural gravel beaches (cf. Austin and Buscombe, 2008).

Fig. 9 demonstrates clearly that XBeach is able to simulate overwash processes with some success. In the final series of XBeach test using the Slapton profile, threshold condition for barrier overwash were investigated by increasing the mean tidal level. The hydrodynamic conditions used in the overwash tests are shown in Fig. 13a. The upper panel shows measured temporal changes in H_s and T_p values measured at 2 km offshore (Fig. 4) at the peak of the storm. These are used in all overwash tests spanning a 6.5 hour tidal period. Tidal levels plus the surge enhancements used in the XBeach simulation (0 m, 1.0 m, 1.4 m, 1.6 m, 2.0 m, 2.2 m and 2.4 m) are shown in the lower panel for the same period. Note that not all are illustrated for clarity. Although it is acknowledged from the outset that surge levels of 2.0 m and 2.4 m are likely to be extremely rare events, surge levels up to 1.4 m are possible, with a return period of approximately 100 years, (cf. Lowe and Gregory, 2005). Tests using these hydrodynamic conditions were undertaken using both the pre-storm and post-storm measured beach profiles in order to assess how pre-established beach morphology affects overwash thresholds. Overwash model results for both cases are shown in Fig. 13b,c. Results from the XBeach simulations using the pre-storm profile (Fig. 13b) showed that with the imposed wave conditions, overwash occurred

Table 3
Brier skill scores for BARDEX tests D2, D3, E8 and E10 using short wave forcing in the XBeach model (Case A). Numbers in brackets in the no reset columns show % difference between reset and no reset tests. Also shown are the mean ($\bar{x}$) and standard deviation (σ_x) values for each test.

Test D2			Test D3		
Run no.	Reset	No reset	Run no.	Reset	No reset
2	0.83	0.76 (8)	2	0.88	0.77 (13)
3	0.79	0.73 (8)	3	0.79	0.64 (19)
4	0.77	0.68 (12)	4	0.75	0.62 (17)
5	0.76	0.62 (18)	5	0.68	0.63 (7)
6	0.69	0.61 (12)	6	0.66	0.57 (14)
7	0.67	0.57 (15)	7	0.65	0.55 (15)
8	0.66	0.53 (20)	8	0.63	0.52 (17)
9	0.67	0.51 (24)	9	0.59	0.48 (19)
10	0.65	0.50 (23)	10	0.61	0.49 (20)
11	0.64	0.49 (23)	11	0.62	0.44 (29)
12	0.66	0.48 (27)	12	0.60	0.42 (30)
13	0.67	0.47 (30)	13	0.58	0.44 (24)
14	0.65	0.48 (26)			
$\bar{x}, \sigma_x$	0.70, (0.06)	0.57, (0.10)	$\bar{x}, \sigma_x$	0.67, (0.09)	0.55, (0.10)
Test E8			Test E10		
2	0.69	0.64 (7)	2	0.57	0.54 (5)
3	0.65	0.56 (14)	3	0.53	0.41 (23)
4	0.63	0.53 (16)	4	0.51	0.31 (39)
5	0.59	0.46 (22)	5	0.42	0.24 (43)
6	0.55	0.44 (20)	6	0.31	0.16 (48)
7	0.56	0.38 (32)	7	0.22	0.08 (64)
8	0.49	0.37 (24)	8	0.09	0.02 (78)
9	0.47	0.33 (30)			
$\bar{x}, \sigma_x$	0.58, (0.08)	0.46, (0.11)	$\bar{x}, \sigma_x$	0.38, (0.18)	0.25, (0.18)

at surge levels of 1.8 m. This is indicated by the arrow showing small washover deposits on the crest of the beach. Storm surge levels required for overwash reduced to approximately 1.2 m when both H_s and T_p were increased by 25% (not illustrated). For the post-storm profile, a surge level of 1.6 m was sufficient to result in the same impact (Fig. 13c). Again increasing H_s and T_p by 25% resulted in overwash when the surge level was only approximately 1.0 m. These results show that gravel beaches in a pre-existing eroded state are

Table 4
Brier skill scores for BARDEX tests D2, D3, E8 and E10 using long wave forcing in the XBeach model (Case B). Numbers in brackets show% difference between short wave and long wave tests.

Test D2 (no reset)			Test D3 (no reset)		
Run no.	Short waves	Long waves	Run no.	Short waves	Long waves
2	0.76	0.72 (5.3)	2	0.77	0.75 (2.6)
3	0.73	0.69 (5.5)	3	0.64	0.61 (4.7)
4	0.68	0.65 (4.4)	4	0.62	0.60 (3.2)
5	0.62	0.60 (3.2)	5	0.63	0.62 (1.6)
6	0.61	0.60 (1.6)	6	0.57	0.56 (1.8)
7	0.57	0.56 (1.8)	7	0.55	0.56 (−1.8)
8	0.53	0.51 (3.8)	8	0.52	0.51 (1.9)
9	0.51	0.52 (−2.0)	9	0.48	0.46 (4.2)
10	0.50	0.49 (2.0)	10	0.49	0.45 (8.2)
11	0.49	0.45 (8.2)	11	0.44	0.41 (6.8)
12	0.48	0.43 (10.4)	12	0.42	0.40 (4.8)
13	0.47	0.42 (10.6)	13	0.44	0.41 (6.8)
14	0.48	0.45 (6.2)			
Test E8 (no reset)			Test E10 (no reset)		
2	0.64	0.62 (3.1)	2	0.54	0.51 (5.6)
3	0.56	0.54 (3.6)	3	0.41	0.39 (4.9)
4	0.53	0.51 (3.8)	4	0.31	0.30 (3.2)
5	0.46	0.42 (8.7)	5	0.24	0.23 (4.2)
6	0.44	0.43 (2.3)	6	0.16	0.14 (6.3)
7	0.38	0.35 (7.9)	7	0.08	0.06 (6.3)
8	0.37	0.36 (2.7)	8	0.02	0.01 (10.0)
9	0.33	0.31 (6.1)			

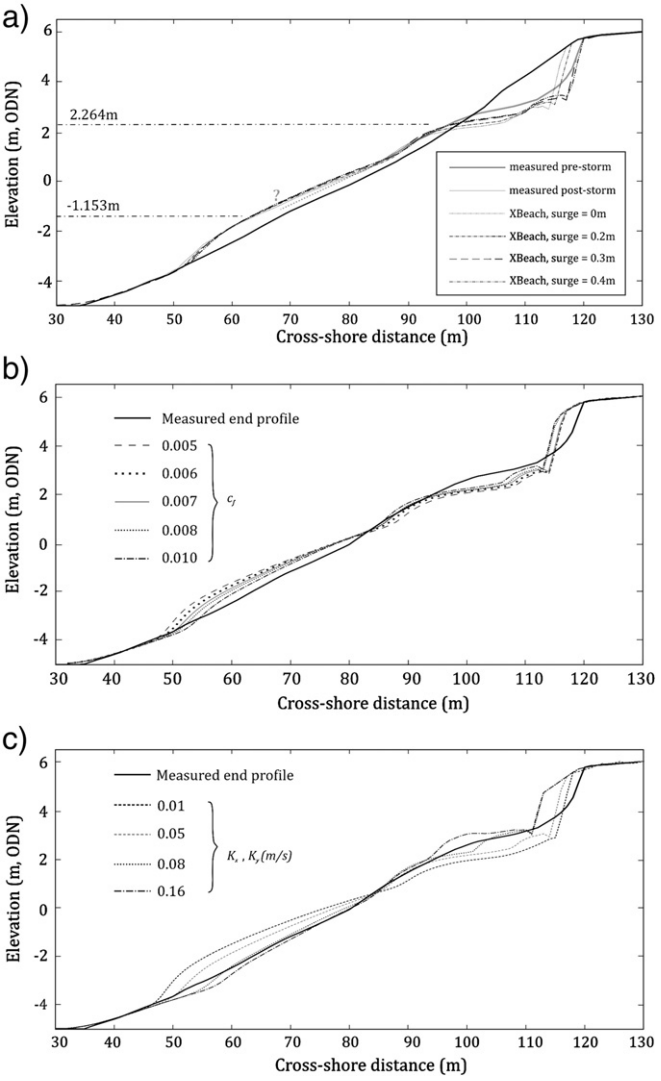

Fig. 10. a) Measured beach profiles at P12 before and after the easterly storm at Slapton for a range of surge enhancements to the mean tidal level. b) Comparison between measured and predicted barrier profile P12 for stated c_f values ($K = 0.05$). c) Comparison between measured and predicted barrier profile P12 for stated K values ($c_f = 0.007$).

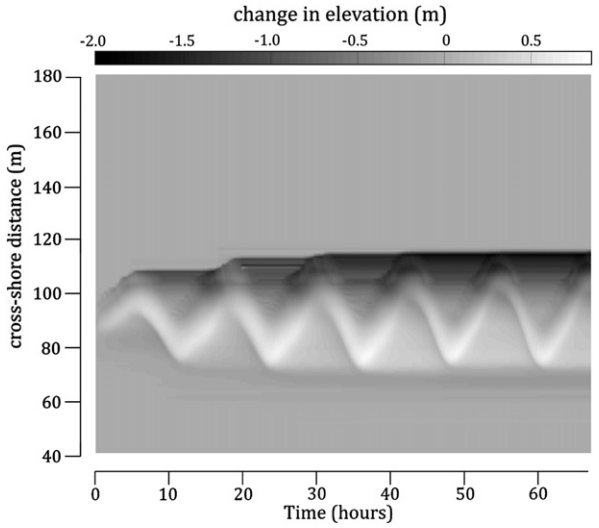

Fig. 11. a) Contoured plot to show temporal and spatial changes in the Slapton beach profile predicted by XBeach during the easterly storm period. b) Temporal changes in elevation of P12 during the easterly storm at Slapton.

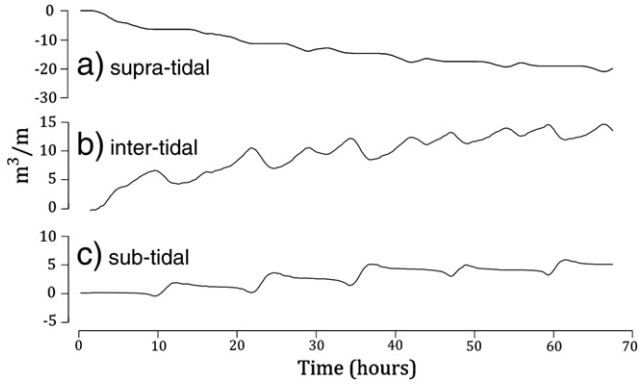

Fig. 12. Changes in beach volume (assuming profile P12 is 1 m wide) for the supra-tidal (2 m to 6.2 m ODN), inter-tidal (−2 m to 2 m ODN) and sub-tidal (−5 m to −2 m ODN) sections of the profile.

more susceptible to further erosion and overwashing should storms occur before a recovery period.

6. Conclusions

Using tidal, short and long wave forcing a 1D version of the XBeach numerical model has been applied in an attempt to replicate measured changes in gravel barrier profile morphology in a range of laboratory experiments and at a field site during a storm.

Irrespective of the wave forcing approach, XBeach simulation of BARDEX experiments was successful provided the starting barrier profile was defined using measured profiles (BSS typically approximately 0.6 for *reset* runs). Using predicted starting profiles (i.e. *no reset* runs), XBeach tended to over-predict erosion on the upper beach face (BSS typically approximately 0.4). In BARDEX overwash tests, XBeach was successful in identifying threshold water level and wave conditions and

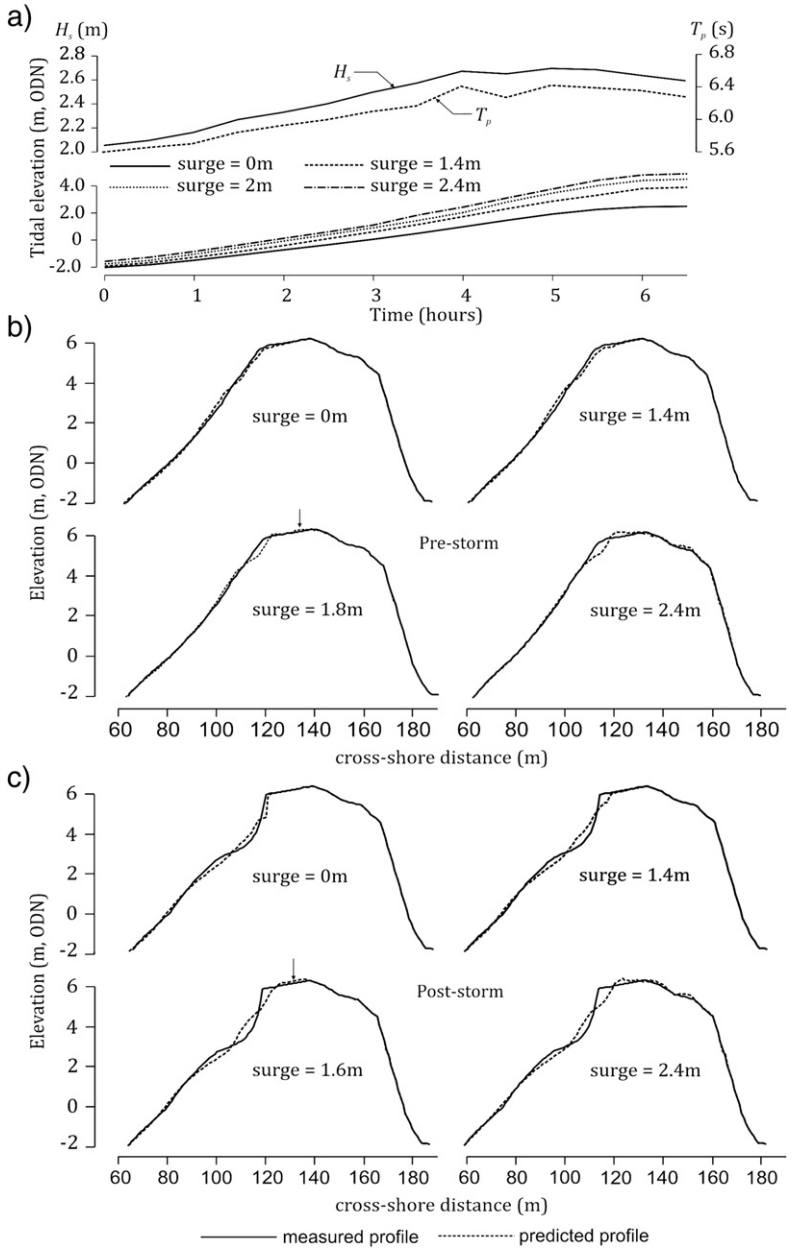

Fig. 13. a) Hydrodynamic conditions used in the Slapton overwash tests. b) Measured and predicted barrier profiles for pre-storm profile overwash simulations. c) Measured and predicted barrier profiles for post-storm profile overwash simulations.

reproduced the majority of the observed morphological change over the barrier crest region with skill. In most cases the use of short waves to drive the XBeach model gave marginally better BSS values. Little difference was detected between XBeach model results using short (i.e. measured incident wave time-series) and long wave (i.e. JONSWAP spectra) forcing at the offshore boundary.

A BSS value of 0.66 demonstrated that XBeach is able to reproduce well the key features of storm-induced supra-tidal erosion and related inter-tidal and sub-tidal accretions at Slapton beach profile P12 using JONSWAP spectra to define incident wave conditions and a storm surge enhancement of 0.4 m on the mean tidal level. An underestimation of changes in the intertidal morphology is thought to be related in part to the exclusion of longshore transport in the XBeach model (cf. Ruiz de Alegria-Arzaburu and Masselink, 2010b). The model was able to reproduce the migration of a step-like feature over a tidal cycle. However, although similar in morphology and behaviour, the feature is thought to be attributable to essentially erosional processes and thus is different from the step found on natural gravel beaches. Despite these uncertainties, the simulation at Slapton demonstrates that XBeach has a good ability to simulate the primary cross-shore morphological responses of a gravel barrier to a storm event.

In both BARDEX and Slapton test cases, the modelled beach profile behaviour showed a strong dependency on beach permeability. This indicates the control on swash infiltration by hydraulic conductivity, and supports the field results reported by Austin (2005) and modelling results by Jamal et al. (2010). Overestimation of K by approximately 30% leads to under-prediction of the post-storm supra-tidal beach volume by approximately 15%, while an under-estimation of K by approximately 20% over-predicts the supra-tidal beach volume by approximately 8%. Using BSS values to identify the best model performance showed that a K value of 0.05 and a drag coefficient value of 0.007 are the most appropriate values to use in the present laboratory and field tests. In all cases the highest BSS values were attained only when groundwater was included in the XBeach simulations reflecting its role as a principal determinant of the rate of infiltration across the beach.

Although the erosional aspect of gravel beach dynamics is handled with moderate success in XBeach, the model does not simulate well the strong up-rush of water that follows wave breaking, and fails to simulate accurately the much weaker backwash attributable to rapid swash infiltration. As a consequence, XBeach is unable to reproduce the formation of the distinct berm observed in BARDEX experiments and in the field. As this feature can provide some additional protection to the upper beach during, for example, a storm event, the present simulations may underestimate threshold conditions for overwash. In this respect model performance might be improved by establishing relationships between the bed shear stresses associated with up-rush and backwash events and the infiltration characteristics across the swash zone. Further, owing to the steep offshore bathymetry associated with gravel beaches, waves break very close to the beach. This has a high impact on gravel beach morphodynamics (cf. Pedrozo-Acuña et al., 2010) and may require special parameterisation in XBeach.

The present work has shown the usefulness of XBeach for establishing barrier overwash thresholds and for simulating storm-induced cross-shore morphological change over time-scales ranging from minutes to days. Both have utility for coastal engineering and beach management.

List of symbols

Roman symbols

A	cross-sectional area to the flow
A_r	roller area
A_{sb}	bed load coefficient
A_{ss}	suspended load coefficient
A_w	wave action
C	actual depth averaged sediment concentration
Cd	drag coefficient
C_{eq}	equilibrium concentration
$C_{g,x}$	wave group velocity in the x-direction
$C_{g,y}$	wave group velocity in the y-direction
C_θ,	velocity in directional space
C_m	time and depth averaged sediment concentration
D	wave energy dissipation
$\bar{D}$	total wave energy dissipation
D_b	expected dissipation rate in a breaking wave
D_h	horizontal diffusion coefficient for sediment
$\bar{D}_r$	roller energy dissipation
D_{waves}	energy dissipation due to wave breaking
D_v	vertical diffusion coefficient for sediment
D_{50}	median grain diameter
D_{90}	grain diameter that 90% of the sediment is finer
D_*	dimensionless particle size
E_{roller}	roller energy
E_w	short wave energy
F	wave and roller force
H	wave height
H_s	significant wave height
H_{rms}	root mean square wave height
K	hydraulic conductivity
L	wavelength
P	pressure drop over distance L
P_b	the fraction of breaking waves
Q	total discharge
S	radiation stress
$Sed_{x,y}$	sediment transport in x and y directions
S_w	wave energy in each directional bin
T	wave period
T_m	mean intrinsic wave period
T_p	peak wave period
T_s	adaptation time scale for sediment
U_m	time and depth averaged flow velocity
X	horizontal distance from the wave paddle
a	flow acceleration
c	actual sediment concentration
c_g	wave group velocity
c_{eq}	equilibrium sediment concentration
c_f	bed friction coefficient
c_m	time averaged sediment concentration
c_w	short wave celerity
f_{morf}	morphological '*acceleration*' term
f_p	peak frequency
f_w	mean intrinsic frequency
g	gravitational acceleration
h	water depth
h_L	'lagoon' depth
h_S	'sea' depth
h_{surge}	residual surge component
k_b	bore-averaged near-bed turbulence
k_w	wave number
n	wave breaking calibration parameter
n_s	directional spreading coefficient
p	sediment porosity
s	relative density (ρ_s/ρ_w)
t	time
u	flow velocity in x-direction
u_A	mean flow component due to nonlinear waves
u_{crit}	critical flow velocity for sediment entrainment
$u_{cr,c}$	critical flow velocity for sediment entrainment due to currents only
$u_{cr,w}$	critical flow velocity for sediment entrainment due to waves only
u_m	time averaged flow velocity

u^E	Eulerian flow velocity in x-direction
$u_{rms,2}$	near-bed short wave orbital motion
u^S	Stokes drift velocity in x-direction
v	flow velocity in y-direction
v^E	Eulerian flow velocity in y-direction
v^S	Stokes drift velocity in y-direction
w_s	sediment fall velocity
x	horizontal cross-shore coordinate
x_b	initial beach profile
x_m	measured beach profile after storm
x_x	beach profile predicted by XBeach
y	horizontal alongshore coordinate
z	vertical coordinate
z_b	bed level
z_0	bed roughness length

Greek symbols

α	calibration factor
α_u	coefficient for time averaged flow due to nonlinear waves, related to the phase shift between intra wave sediment suspension and flow
β	beach slope
β_w	slope of the wave front
γ	wave breaking calibration parameter
γ_c	bed calibration coefficient for near-bed sediment concentration
γ_{flow}	flow calibration factor in equilibrium sediment concentration
γ_{morf}	bed level multiplication factor
γ_j	peak spectral enhancement factor
γ_{turb}	turbulence calibration factor in equilibrium sediment concentration
γ_{visc}	calibration factor (≈ 1.0)
η	water surface elevation
κ	beach permeability
μ	dynamic viscosity
ν_h	horizontal viscosity
ν_w	vertical viscosity
θ	wave angle
θ_w	mean wave angle
ρ_s	mass density of sand
ρ_w	mass density of water
τ_w	wave period-averaged shear stress
ω	intrinsic radian wave frequency

Acknowledgements

The data reported here were collected in the Delta flume (Netherlands) as part of the EU-funded BARDEX project (HYDRALAB III Contract no. 022441 (RII3), Barrier Dynamics Experiments).

Appendix A. The XBeach model[5]

In the 2D co-ordinate system of XBeach the computational x-axis is always oriented towards the coast, and the y-axis is directed alongshore and is defined relative to world coordinates (x_w, y_w) through the origin (x_{ori},y_{ori}) and the orientation α_0, defined counter-clockwise with relation to the x_w-axis. The grid applied is rectilinear, non-equidistant and staggered. Bed levels, water levels, water depths and sediment concentrations are defined in cell centres. Velocity and sediment transport are defined in u- and v-points, located at the cell interfaces. In the wave model, wave action, roller energy and radiation stresses are defined in cell centres, whereas radiation stress gradients are defined at u- and v-points. Here we give the equations in the XBeach model for the 1D cases considered in this paper.

Taking account of the directional distribution of the short wave action density, and assuming a narrow banded incident spectrum (cf. Holthuijsen et al., 1989), a solution to the time-dependent short wave action balance is obtained on the *scale of wave groups* by reducing the frequency domain to a single representative peak frequency. This simplifying approach provides computationally efficient solutions for time-varying currents and directionally-spread infragravity waves. The wave action balance is given as

$$\frac{\partial A_w}{\partial t}+\frac{\partial c_{g,x}A_w}{\partial x}+\frac{\partial c_{g,y}A_w}{\partial y}+\frac{\partial c_\theta Aw}{\partial \theta}=-\frac{D}{\omega} \tag{A1}$$

where the wave action $A_w = E_w/\omega$, E_w is the wave energy, ω is the intrinsic wave frequency and D is the wave dissipation. The x- and y-group velocities (i.e. $C_{g,x} = c_g \cos(\theta)$, $C_{g,y} = c_g \sin(\theta)$) represent the respective components of the wave group velocity, c_g. The term C_θ, expressing the propagation speed in θ-space, takes into account refraction due to bed interactions so that

$$C_\theta=\frac{\omega}{\sinh 2k_w h}\left(\frac{\partial h}{\partial x}\sin\theta-\frac{\partial h}{\partial y}\cos\theta\right). \tag{A2}$$

Here h is the water depth and the wave number k_w is derived from the linear dispersion equation:

$$\omega=\sqrt{gk_w\tan hk_w h};\ \text{and} \tag{A.3}$$

$$c_g=c_w\left(\frac{1}{2}+\frac{k_w h}{\sinh 2k_w h}\right). \tag{A.4}$$

The energy dissipation due to wave breaking, D, is modelled using the approach of Roelvink (1993). Here the total dissipation, $\bar{D}$, is defined as

$$\bar{D}=0.25\propto\rho_w P_b f_m\frac{H_{rms}^3}{h} \tag{A5}$$

where α is a calibration factor $O(1)$, ρ_w is the water density, g is the acceleration due to gravity, f_w is the mean intrinsic frequency, H_{rms} is the root mean square wave height and P_b is the fraction of breaking waves defined as

$$P_b=1-\exp\left[-\left(\frac{H_{rms}}{\gamma h}\right)^n\right] \tag{A6}$$

where γ and n are calibration factors $O(0.5)$ and $O(10)$, respectively and H_{rms} is computed from the short wave energy using

$$H_{rms}=\sqrt{\frac{8E_w}{\rho_w g}},\quad \text{where}\quad Ew=\int_0^{2\pi}S_w d\theta \tag{A7}$$

and $\bar{D}$ is distributed over all wave directions using

$$D=\frac{Sw}{Ew}\bar{D}. \tag{A8}$$

Radiation stresses are then obtained from:

$$S_{xx}=\int\left[\frac{c_g}{c_w}\left(1+\cos^2\theta\right)-\frac{1}{2}\right]S_w d\theta; \tag{A9}$$

$$S_{xy}=S_{yx}=\int\sin\theta\cos\theta\left(\frac{c_g}{c_w}s_w\right)d\theta;\ \text{and} \tag{A10}$$

[5] The model description in this Appendix is derived from: Van Thiel de Vries (2009).

$$Syy = \int \left[\frac{c_g}{c_w}\left(1 + \sin^2\theta\right)\frac{1}{2}\right] S_w d\theta. \tag{A11}$$

Using the dissipation of short wave energy as a source term in a roller energy balance equation, XBeach is able to redistribute energy from breaking waves using

$$\frac{\partial E_{roller}}{\partial t} + \frac{\partial c_{w,x} E_{roller}}{\partial x} + \frac{\partial c_{w,y} E_{roller}}{\partial y} + \frac{\partial c_\theta E_{roller}}{\partial \theta} = -D_{roller} + D \tag{A12}$$

where E_{roller} is the roller energy in each directional bin. The roller energy propagation speeds are defined in terms of the short wave celerity c_w as $c_{w,x} = c_w \cos(\theta)$ and $c_{w,y} = c_w \sin(\theta)$, and roller dissipation is given by $\overline{D}_r? = c_w \tau_w$, (Deigaard, 1993). The term τ_w represents the wave period-averaged shear stress between the roller and the water surface and is defined using the slope of the wave front, β_w, and wavelength, L, as

$$\tau_r \frac{\rho_w g A_r \sin(\beta_w)}{L} \tag{A13}$$

where A_r is the roller area (Reniers, 1999). Following Svendsen (1984), roller energy is given by

$$E_{roller} = \frac{1}{2}\frac{\rho_w A_r c_w^2}{L}, \quad \text{where} \quad E_{roller} \int_0^{2\pi} S_r d\theta. \tag{A14}$$

Thus

$$\bar{D}_r = \frac{2g \sin(\beta_w) E_r}{C_w} \tag{A15}$$

where β_w is calculated with a wave shape model (Van Thiel de Vries, 2009), and $\bar{D}_r$ is distributed proportionally over all wave directions to give

$$D_r = \frac{S_r}{E_{roller}} \bar{D}_r. \tag{A16}$$

The contribution to radiation stress by rollers is then added to the wave-induced radiation stress using:

$$S_{xx,r} = \int \cos^2\theta S_r d\theta; \tag{A17}$$

$$S_{xy,r} = S_{yx} = \int \sin\theta \cos\theta S_r d\theta; \text{and} \tag{A18}$$

$$S_{yy,r} = \int \sin^2\theta S_w d\theta. \tag{A19}$$

The resulting wave forcing is then given by:

$$F_x = -\left(\frac{\partial S_{xx}}{\partial x}\right); \text{ and} \tag{A20}$$

In XBeach the wave energy balance, the roller energy and radiation stress are defined at the cell centres, and the radiation stress gradients are defined at u- and v-points. Surface elevation and flow, including infragravity waves and unsteady wave-induced currents, are solved using the shallow water momentum and mass balance equations. To include short wave-induced mass fluxes and return flows in shallow water, XBeach uses the Generalized Lagrangian Mean (GLM) formulation (Andrews and McIntyre, 1978). Here Lagrangian equivalents, u^L and v^L, are defined as

$$u^L = u^E + u^S \text{ and } v^L = v^E + v^S \tag{A21}$$

where the Stokes drift terms in the x- and y-directions are given by Phillips (1977) in the form

$$u^S = \frac{(E_w + 2E_r)\cos\theta}{\rho_w h c_w} \text{ and } v^S = \frac{(E_w + 2E_r)\sin\theta}{\rho_w h c_w}. \tag{A22}$$

In the present study the depth-average GLM-shallow water equations are expressed as:

$$\frac{\partial u^L}{\partial t} + u^L\frac{\partial u^L}{\partial x} + v^L\frac{\partial u^L}{\partial y} - \nu_h\left(\frac{\partial^2 u^L}{\partial x^2} + u^L\frac{\partial^2 u^L}{\partial y^2}\right) = -g\frac{\partial \eta}{\partial x} - \frac{C_f u^E\sqrt{(1.16u_{rms})^2 + (u^E)^2 + (v^E)^2}}{h} + \frac{F_x}{\rho_s h}; \tag{A23}$$

$$\frac{\partial v^L}{\partial t} + v^L\frac{\partial v^L}{\partial x} + u^L\frac{\partial v^L}{\partial y} - \nu_h\left(\frac{\partial^2 v^L}{\partial y^2} + u^L\frac{\partial^2 v^L}{\partial x^2}\right) = -g\frac{\partial \eta}{\partial y} - \frac{C_f v^E\sqrt{(1.16u_{rms})^2 + (u^E)^2 + (v^E)^2}}{h} + \frac{F_y}{\rho_s h}; \text{ and} \tag{A24}$$

$$\frac{\partial \eta}{\partial t} + \frac{\partial u^L h}{\partial x} + \frac{\partial v^L h}{\partial y} = 0. \tag{A25}$$

Here L- and E-indices for the x (u) and y (v) velocities refer to Lagrangian and Eulerian framework, η is the water surface elevation, c_f is the bed friction coefficient (equivalent to the drag coefficient, Cd), F_x and F_y are the wave and roller forces and ν_h is the horizontal viscosity coefficient (modified by wave breaking in the surf zone), (cf. Reniers et al., 2004). Bed friction is calculated using the parameterisation of Feddersen et al. (2000) using both the Eulerian flow velocities (u^E,v^E) and the short wave orbital velocity, calculated using

$$u_{rms} = \frac{\pi H}{T\sqrt{2\sinh(kh)}} \tag{A26}$$

where the wave height $H = \sqrt{{}^8E/_{\rho g}}$, and T is the wave period.

Sediment transport is modelled using a depth-averaged advection–diffusion scheme with a source-sink term based on an equilibrium sediment concentration (e.g. Galapatti and Vreugdenhil, 1985). This takes the form

$$\frac{\partial hC}{\partial t} + \frac{\partial hC\left(u^E + u_a \sin\theta m\right)}{\partial x} + \partial hC\frac{\mathbb{I}\left(v\right]^E + u_a\cos\theta m\right)}{\partial y} + \frac{\partial}{\partial x}\left(D_s h\frac{\partial C}{\partial x}\right) + \frac{\partial}{\partial y}\left(D_s h\frac{\partial C}{\partial y}\right) = \frac{hC_{eq} - hC}{T_s} \tag{A27}$$

where C represents the depth-averaged concentration (on the wave group scale), u_a is a flow velocity related to wave nonlinearity (Van Thiel de Vries, 2009), θ_m is the mean angle of the incoming waves, T_s is the sediment concentration adaptation time-scale. This is computed using a simple expression based on local water depth and particle settling velocity, w_s in the form

$$T_s = \max\left(\frac{h}{w_s}, T_{s,min}\right) \tag{A28}$$

where $T_{s,min}$ is a user-specified minimum adaptation time. For small values of h, $T_s \approx T_{s,min}$ forcing sediment concentration to respond instantaneously with local hydrodynamic conditions. The erosion or accretion of

sediment is determined by the difference between the actual sediment concentration C and the equilibrium concentration C_{eq}.

References

Andrews, D.G., McIntyre, M.E., 1978. An exact theory of nonlinear waves on a Lagrangian-mean flow. Journal of Fluid Mechanics 89 (4), 609–646.

Austin, M. J., 2005. Swash, groundwater and sediment transport processes on a gravel beach. Unpub. PhD thesis, Loughborough Univ.

Austin, M.J., Buscombe, D., 2008. Morphological change and sediment dynamics of the beach step on a macrotidal gravel beach. Marine Geology 249, 167–183.

Austin, M.J., Masselink, G., 2005. Infiltration and exfiltration on a steep gravel beach: implications for sediment transport. Proc. Coastal Dynamics 2005. doi:10.1061/40855(214)102.

Austin, M.J., Masselink, G., 2006. Swash-groundwater interaction on a steep gravel beach. Continental Shelf Research 26 (20), 2503–2519.

Austin, M., Masselink, G., Turner, I., Buscombe, D., Williams, J., 2009. Groundwater seepage between a gravel barrier beach and a freshwater lagoon. In: Smith, J.M. (Ed.), Proc. Coastal Eng. 2008: ASCE, 5, pp. 4572–4584.

Bosboom, J., Aarninkhof, S.G.J., Reniers, A.J.H.M., Roelvink, J.A., Walstra, D.J.R., 2000. UNIBEST-TC 2.0 — Overview of Model Formulations, Rep. H2305. Delft Hydraulics, Delft, p. 42.

Bradbury, A.P., 2000. Predicting breaching of shingle barrier beaches — recent advances to aid beach management. Proc. 35th MAFF (Defra) Conf. on River and Coastal Eng. , pp. 05.3.1–05.3.13.

Bradbury, A., Powell, K.A., 1992. The short-term profile response of shingle spits to storm wave action. Proc. 23rd Int. Conf. Coastal Eng. , pp. 2694–2707.

Bradbury, A., Cope, S.N., Prouty, D.B., 2005. Predicting the response of shingle barrier beaches under extreme wave and water level conditions in Southern England. Proceedings of Coastal Dynamics. doi:10.1061/40855(214)94.

Bradbury, A., Stratton, M., Mason, T., 2011. Impacts of wave climate with bi-modal wave period on the profile response of gravel beaches. In: Wang, P., Rosati, J.D., Roberts, T.M. (Eds.), Proc. Coastal Sediments 2011, Vol. 3. World Scientific, pp. 2004–2018.

Chadwick, A.J., 1989. Field measurements and numerical model verification of coastal shingle transport. BHRA, 27. the Fluid Eng. Centre, Cranfield, Bedford.

Clark, S., Damgaard, J., 2002. Application of a numerical model of swash zone flow on gravel beaches. Proc. 28th Int. Conf. Coastal Eng. ASCE, pp. 1028–1036.

Clark, S., Dodd, N., Damgaard, J., 2004. Modeling flow within and above a porous beach. Journal of Waterway, Port, Coastal, and Ocean Engineering 130, 223–233.

Davidson, M.A., Lewis, R., Turner, I., 2010. Forecasting seasonal to multi-year shoreline change. Coastal Engineering. doi:10.1016/j.coastaleng.2010.02.001.

Deigaard, R., 1993. A note on the three-dimensional shear stress distribution in a surf zone. Coastal Engineering 20, 157–171.

Donnelly, C., Kraus, N., Larson, M., 2006. State of knowledge on measurement and modeling of coastal overwash. Journal of Coastal Research 22 (4), 965–991.

Feddersen, F., Guza, R.T., Elgar, S., Herbers, T.H.C., 2000. Velocity moments in alongshore bottom stress parameterizations. Journal of Geophysical Research 105 (C4), 8673–8686.

Galapatti, R., 1983. A depth-integrated model for suspended transports. Report 83-7. Faculty of Civil Eng., Delft Univ. of Tech., Delft, The Netherlands.

Galapatti, R., Vreugdenhil, C.B., 1985. A depth-integrated model for suspended sediment transport. Journal of Hydraulic Research 23 (4), 359–377.

Guza, R.T., Thornton, E.B., Holman, R.A., 1984. Swash on steep and shallow beaches. Proc. 19th Int. Conf. Coastal Eng. ASCE, Houston, Texas, pp. 708–723.

Holthuijsen, L.H., Booij, N., Herbers, T.H.C., 1989. A prediction model for stationary, short-crested waves in shallow water with ambient currents. Coastal Engineering 13, 23–54.

Hughes, S.A., 1993. Laboratory wave reflection analysis using co-located gauges. Coastal Engineering 20, 223–247.

Jamal, M.H., Simmonds, D.J., Magar, V., Pan, S., 2010. Modelling infiltration on gravel beaches with an XBeach variant. Proc.32nd Conf. on Coastal Eng., Shanghai, China, 2010, sediment, p. 41http://journals.tdl.org/ICCE/issue/view/154/showToc.

Kleinhans, M.G., Van Rijn, L.C., 2002. Stochastic prediction of sediment transport in sand–gravel bed rivers. Journal of Hydraulic Engineering 128, 412–425.

Komar, P.D., Miller, M.C., 1975. On the comparison between the threshold of sediment motion under waves and unidirectional currents with a discussion of the practical evaluation of the threshold. Journal of Sedimentry Petrology 45, 362–367.

Kubota, S., Mizuguchi, M., Takezawa, M., 1990. Reflection from swash zone on natural beaches. Proc. 22nd Coastal Eng. Conf. ASCE, Reston VA, USA, pp. 570–583.

Larson, M., Kraus, N., 1989. SBEACH: numerical model for simulating storm induced beach change. Report 1, Empirical Foundation and Model Development, Tech. Rept. CERC-89-9. US Army Eng. Waterways Exp. Station, Vicksburg, MS. (267 pp.).

Lawrence, J., Chadwick, A.J., Flemming, C., 2001. A phase resolving model of sediment transport on coarse grained beaches. Proc. 27th Int. Conf. Coastal Eng. ASCE, pp. 624–636.

Lawrence, J., Karunarathna, H., Chadwick, A.J., Flemming, C., 2002. Cross-shore sediment transport on mixed coarse grain sized beaches: modelling and measurements. Proc. 28th Int. Conf. Coastal Eng. ASCE, pp. 2565–2577.

López de San Roman-Blanco, B., Coates, T.T., Holmes, P., Chadwick, A.J., Bradbury, A., Baldock, T.E., Pedrozo-Acuña, A., Lawrence, J., Grüne, J., 2006. Large Wave Channel (GWK) experiments on gravel and mixed beaches: experimental procedure and data documentation. Coastal Engineering 4, 349–362.

Lorang, M.S., 2002. Predicting the crest height of a gravel beach. Geomorphology 48, 87–101.

Lowe, J.A., Gregory, J.M., 2005. The effects of climate change on storm surges around the united kingdom. Philosophical Transactions of the Royal Society A: Mathematical, Physical & Engineering Sciences 363 (1831), 1313–1328.

Mason, T., Coates, T.T., 2001. Sediment transport processes on mixed beaches: a review for shoreline management. Journal of Coastal Research 17 (3), 645–657.

Masselink, G., Li, L., 2001. The role of swash infiltration in determining the beachface gradient: a numerical study. Marine Geology 176, 139–156.

Masselink, G., Russell, P., Blenkinsopp, C., Turner, I., 2010. Swash zone sediment transport, step dynamics and morphological response on a gravel beach. Marine Geology. doi:10.1016/j.margeo.2010.03.005.

McCall, R.T., Van Thiel de Vries, J.S.M., Plant, N.G., Van Dongeren, A.R., Roelvink, J.A., Thompson, D.M., Reniers, A.J.H.M., 2010. Two-dimensional time dependent hurricane overwash and erosion modelling at Santa Rosa Island. Coastal Eng. 57 (7), 668–683.

Nairn, R.B., Roelvink, J.A., Southgate, N.H., 1990. Transition zone width and implications for modelling surf zone hydrodynamics. 22th Int. Conf. Coastal Eng., Delft, The Netherlands, pp. 68–81.

Obhrai, C., Powell, K., Bradbury, A., 2008. A laboratory study of overtopping and breaching of shingle barrier beaches. Proc. Coastal Eng. ASCE, Hannover, Germany, pp. 1497–1508.

Packwood, A.R., 1983. The influence of beach porosity on wave uprush and backwash. Coastal Engineering 7, 29–40.

Pedrozo-Acuna, A., Simmonds, D.J., Chadwick, A.J., Silva, R., 2007. A numerical–empirical approach for evaluating morphodynamic processes on gravel and mixed sand–gravel beaches. Marine Geology 241 (1–4), 1–18.

Pedrozo-Acuña, A., Torres-Freyermuth, A., Zou, Q., Hsu, T.-J., Reeve, D.E., 2010. Diagnostic modelling of impulsive pressures induced by plunging breakers. Coastal Engineering 57 (3), 252–266.

Pedrozo-Acuña, A., Simmonds, D.J., Otta, A.K., Chadwick, A.J., 2006. On the crossshore profile change of gravel beaches. Coastal Engineering 53 (4), 335–347.

Peregrine, D.H., 1972. Equations for water waves and the approximations behind them. In: Meyer, R.E. (Ed.), Waves on Beaches and Resulting Sediment Transport. Academic Press, pp. 95–122.

Phillips, O.M., 1977. The Dynamics of the Upper Ocean. Cambridge Univ., Press, New York. (336 pp.).

Powell, K.A., 1990. Predicting short term profile response for shingle beaches. HR Wallingford Rept, SR219. .

Pye, K., 2001. The nature and geomorphology of coastal shingle. In: Packham, J.R., Randall, R.E., Barnes, R.S.K., Neal, A. (Eds.), Ecology and Geomorphology of Coastal Shingle. Westbury Academic Publ., pp. 2–22.

Pye, K., Blott, S.J., 2009. Progressive breakdown of a gravel-dominated coastal barrier, Dunwich–Walberswick, Suffolk, UK: processes and implications. Journal of Coastal Research 25 (3), 589–602.

Reniers, A.J.H.M., 1999. Longshore Current Dynamics. Delft Univ. Tech, Delft.

Reniers, A.J.H.M., Roelvink, J.A., Thornton, E.B., 2004. Morphodynamic modeling of an embayed beach under wave group forcing. Journal of Geophysical Research 109 (C01030).

Roelvink, J.A., 1993. Dissipation in random wave groups incident on a beach. Coastal Engineering 19, 127–150.

Roelvink, J.A., Stive, M.J.F., 1989. Bar-generating cross-shore flow mechanisms on a beach. Journal of Geophysical Research 94 (C4), 4785–4800.

Roelvink, J.A., Reniers, A., van Dongeren, A., de Vries, J., McCall, R., Lescinski, J., 2009. Modelling storm impacts on beaches, dunes and barrier islands. Coastal Engineering 56 (11–12), 1133–1152.

Roelvink, D., Reniers, A., Van Dongeren, A., De Vries, J.V.T., Lescinski, J., McCall, R., 2010. XBeach Model description and Manual. Unesco-IHE Institute for Water Education, Deltares and Delft University of Tecnhology. Report June, 21 2010 version 6.

Ruiz de Alegria-Arzaburu, A., Masselink, G., 2010a. Storm response and beach rotation on a gravel beach, Slapton Sands, U.K Marine Geology 278, 77–99. doi:10.1016/j.margeo.2010.09.004.

Ruiz de Alegria-Arzaburu, A., Pedrozo-Acuna, A., Horrillo-Caraballo, J.M., Masselink, G., Reeve, D.E., 2010b. Determination of wave-shoreline dynamics on a macrotidal gravel beach using Canonical Correlation Analysis. Coastal Engineering 57, 290–303.

Soulsby, R., 1997. Dynamics of Marine Sands. Thomas Telford Publ., London.

Soulsby, R.L., Damgaard, J.S., 2005. Bedload sediment transport in coastal waters. Coastal Engineering 52 (8), 673–689.

Srinivas, R., Dean, R.G., 1996. Cross-shore hydrodynamics and profile response modeling. Coastal Engineering 27, 195–221.

Stive, M.J.F., Dingemans, M.W., 1984. Calibration and Verification of a One Dimensional Wave Energy Decay Model. Delft Hydraulics, Delft, The Netherlands.

Stive, M.J.F., Wind, H.G., 1986. Cross-shore mean flow in the surf zone. Coastal Engineering 10, 325–340.

Stockdon, H.F., Sallenger, A.H., Holman, R.A., Howd, P.A., 2007. A simple model for the spatially-variable coastal response to hurricanes. Marine Geology 238, 1–20.

Sutherland, J., Peet, A.H., Soulsby, R.L., 2004. Evaluating the performance of morphological models. Coastal Engineering 51 (8–9), 917–939.

Svendsen, I.A., 1984. Wave heights and set-up in a surf zone. Coastal Engineering 8, 303–329.

Tatavarti, R.V., Huntley, D.A., Bowen, A.J., 1988. Incoming and outgoing wave interactions on beaches. Proc. 21st Coastal Eng. Conf. ASCE, Reston VA, USA, pp. 136–150.

Tuan, T.Q., Verhagen, H.J., Visser, P.J., Stive, M.J.F., 2006. Wave overwash at low-crested beach barriers. Coastal Engineering 48 (4), 371–393.

Van der Meer, J.W., 1988. Rock slopes and gravel beaches under wave attack. Ph.D.Thesis, Delft Univ. of Tech., Delft, The Netherlands.

Van Dongeren, A.R., Svendsen, I.A., 1997. Absorbing-generating boundary condition for shallow water models. Journal of Waterway, Port, Coastal, and Ocean Engineering 123 (6), 303–313.

Van Dongeren, A.R., Reniers, A.J.H.M., Battjes, J.A., 2003. Numerical modelling of infragravity waves response during DELILAH. Journal of Geophysical Research 108 (C9), 3288. doi:10.1029/2002JC001332.

Van Rijn, L.C., 1993. Principles of sediment transport in rivers, estuaries and coastal seas. Part I, Edition 1993. Aqua Pub., Amsterdam.

Van Rijn, L.C., 2007. Unified view of sediment transport by currents and waves, parts I, II, III and IV. Journal of Hydraulic Engineering 133 (6, 7), 649–689 ((part I &II), 761–793 (part III & IV)).

van Rijn, L.C., Walstra, D.J.R., Grasmeijer, B., Sutherland, J., Pan, S., Sierra, J.P., 2003. The predictability of cross-shore bed evolution of sandy beaches at the time scale of storms and seasons using process-based profile models. Coastal Engineering 47 (3), 295–327.

Van Thiel de Vries, J.S.M., 2009. Dune erosion during storm surges. PhD thesis, IOS Press, The Netherlands, ISBN: 978-1-60750-041-4, 200 pp.

Van Wellen, E., Chadwick, A.J., Mason, T., 2000. A review and assessment of longshore sediment transport equations for coarse grained beaches. Coastal Engineering 40 (3), 243–275.

Walstra, D.J.R., Roelvink, J.A., Groeneweg, J., 2000. Calculation of wave-driven currents in a 3D mean flow model. 27th Int. Conf. Coastal Eng. ASCE, Sydney, pp. 1050–1063.

Walton, T.L., 1992. Wave reflection from natural beaches. Ocean Engineering 19, 239–258.